A Theory for Turbulent Pipe and Channel Flows

By WILLIAM K GEORGE,
LUCIANO CASTILLO AND MARTIN WOSNIK
State University of New York at Buffalo, Buffalo, NY 14260 USA

(Received 17 November 1997)

A theory for turbulent pipe and channel flows is proposed which extends the classical analysis to include the effects of finite Reynolds number. The proper scaling for these flows at finite Reynolds number is developed from dimensional and physical considerations using the Reynolds-averaged Navier-Stokes equations. In the limit of infinite Reynolds number, these reduce to the familiar law of the wall and velocity deficit law respectively.

The fact that both the scaled profiles describe the entire flow for finite values of Reynolds number but reduce to inner and outer profiles is used to determine their functional forms in the "overlap" region which both retain in the limit. This overlap region corresponds exactly to the constant Reynolds shear stress region ($30 < y^+ < 0.1R^+$ approximately where $R^+ = u_* R/\nu$). The profiles in this overlap region are logarithmic, *but* in the variable $y + a$ where a is an offset. Unlike the classical theory, the additive parameters, B_i, B_o, and log coefficient, $1/\kappa$, depend on R^+, They are asymptotically constant, however, and are linked by a constraint equation. The corresponding friction law is also logarithmic and entirely determined by the velocity profile parameters, or *vice versa.*

It is also argued that there exists a *mesolayer* near the bottom of the overlap region approximately bounded by $30 < y^+ < 300$ where there is not the necessary scale separation between the energy and dissipation ranges for inertially-dominated turbulence. As a consequence, the Reynolds stress and mean flow retain a Reynolds number dependence, even though the terms explicitly containing the viscosity are negligible in the single-point Reynolds averaged equations. A simple turbulence model shows that the overlap parameter a accounts for the mesolayer, and because of it a logarithmic behavior in y applies only beyond $y^+ > 300$, well outside where it has commonly been sought.

The experimental data from the superpipe experiment and DNS channel flow are carefully examined and shown to be in excellent agreement with the new theory over the entire range from $1.8 \times 10^2 < R^+ < 5.3 \times 10^5$. The Reynolds number dependence of all the parameters and the friction law can be determined from the single empirical function, $H = A/(\ln R^+)^\alpha$, just as for boundary layers. The Reynolds number dependence of the parameters dies off very slowly with increasing Reynolds number, and the asymptotic behavior is reached only when $R^+ >> 10^5$.

---

† This paper was prepared for *Disquisitiones Mechanicae* at the University of Illinois, Department of Theoretical and Applied Mechanics, Urbana, Ill, Oct 24-26, 1996.

CONTENTS

1. Introduction

Pipe and channel flows have recently become the subject of intense scrutiny, thanks in part to new experimental data which has become available from the superpipe experiment at Princeton (Zagarola and Smits 1996, Zagarola 1996). In spite of the facts that the scaling laws were established for pipes and channels more than 80 years ago (Stanton and Pannell 1914, Prandtl 1932) and that the now classical theory of Millikan was offered in 1938 for the friction law and velocity profiles, the subject has remained of considerable interest. Examples from the last 30 years alone include the analyses of Tennekes (1968), Bush and Fendell (1974), Long and Chen (1981), and Panton (1990). All of these were essentially refinements on the original Millikan theory in which the essential functional form of the friction and velocity laws was logarithmic, and only the infinite Reynolds number state was considered. The difficulties presented by the experimental data have recently been extensively reviewed by Gad-el-Hak and Bandyopadhyay (1994).

Barenblatt (1978, 1993) has suggested that the velocity profiles of pipe, channel and boundary layer flows were power laws. In contrast, George and his coworkers (George and Bower 1988; George 1990, 1995; George and Castillo 1993, 1997; George et al. 1992, 1996) have argued that the overlap velocity profile and friction law for boundary layers are power laws, but that the corresponding relations for pipes and channels are logarithmic.

Specifically, George and Castillo (1997) used the Reynolds-averaged Navier-Stokes equations and an Asymptotic Invariance Principle to deduce that the proper scaling velocity for the outer part of the boundary layer was U_∞, the free stream velocity. In the inner region, however, the proper scale velocity was u_*, the friction velocity, just as in the classical Law of the Wall. Since the ratio of u_*/U_∞ varied with Reynolds number, so did the velocity profiles in the *Reynolds number dependent* overlap region. These were derived using Near-Asymptotics as

$$\frac{U}{u_*} = C_i(y^+ + a^+)^\gamma \tag{1.1}$$

and

$$\frac{U - U_\infty}{U_\infty} = C_o(\overline{y} + \overline{a})^\gamma \tag{1.2}$$

where $y^+ = y/\eta, \eta = \nu/u_*$, $\overline{y} = y/\delta$ where δ is the boundary layer thickness (chosen as $\delta_{0.99}$ for convenience). This overlap region was shown to correspond exactly to the region of approximately constant Reynolds stress region of the flow, $30 < y^+ < 0.1\delta^+$.

The parameter a represents an origin shift, and was shown to be related to the existence of a mesolayer in the region approximately given by $30 < y^+ < 300$ in which the dissipative scales are not fully separated from the energy and Reynolds stress producing ones. The parameters C_i, C_o, and γ were functions of δ^+, asymptotically constant, and satisfied the constraint equation,

$$\ln \delta^+ \frac{d\gamma}{d\ln \delta^+} = \frac{d \ln C_o/C_i}{d \ln \delta^+} \tag{1.3}$$

where $\delta^+ = u_* \delta/\nu$. The friction law was given by

$$\frac{u_*}{U_\infty} = \frac{C_o}{C_i} \delta^{+-\gamma} \tag{1.4}$$

The constraint equation was transformed by defining a single new function $h = h(\ln \delta^+)$ so that

$$\ln C_o/C_i = (\gamma - \gamma_\infty) \ln \delta^+ + h \tag{1.5}$$

and

$$\gamma - \gamma_\infty = -\frac{dh}{d \ln \delta^+} \tag{1.6}$$

The function $h - h_\infty$ was determined empirically to be given by

$$h(\delta^+) - h_\infty = \frac{A}{(\ln \delta^+)^\alpha} \tag{1.7}$$

where $h_\infty = \ln(C_{o\infty}/C_{i\infty})$ and $\alpha > 1$ is a necessary condition.

It followed immediately that

$$\gamma - \gamma_\infty = \frac{\alpha A}{(\ln \delta^+)^{1+\alpha}} \tag{1.8}$$

$$\frac{C_o}{C_i} = \frac{C_{o\infty}}{C_{i\infty}} \exp[(1+\alpha)A/(\ln \delta^+)^\alpha] \tag{1.9}$$

and

$$\frac{u_*}{U_\infty} = \frac{C_{o\infty}}{C_{i\infty}} (\delta^+)^{-\gamma_\infty} \exp[A/(\ln \delta^+)^\alpha] \tag{1.10}$$

The values for the constants were determined from the data to be $\gamma_\infty = 0.0362$, $C_{o\infty}/C_{i\infty} = \exp(h_\infty) = 0.0164$, $C_o \approx C_{o\infty} = 0.897$ (so $C_{i\infty} = 55$), $A = 2.91$, and $\alpha = 0.46$. Also it was established from the available data that a^+ was nearly constant and approximately equal to -16.

The purpose of this paper is to apply the same methodology to pipe and channel flows, and to compare the resulting theory with the new experimental data. The important difference from previous efforts mentioned above will be seen to be that the effects of finite Reynolds number are explicitly included and the mesolayer is accounted for.

2. Scaling Laws for Turbulent Pipe and Channel Flow

The stream-wise momentum equation for a fully developed two-dimensional channel flow at high Reynolds number reduces to

$$0 = -\frac{1}{\rho}\frac{dP}{dx} + \frac{\partial}{\partial y}\left[< -uv > + \nu \frac{\partial U}{\partial y}\right] \tag{2.1}$$

Like the boundary layer, the viscous term is negligible everywhere except very near the

wall, so that the core (or outer) flow in the limit of infinite Reynolds number is governed by

$$0 = -\frac{1}{\rho}\frac{dP}{dx} + \frac{\partial}{\partial y} < -uv > \tag{2.2}$$

In the limit of infinite Reynolds number, the inner layer is governed by

$$0 = \frac{\partial}{\partial y}\left[< -uv > +\nu\frac{\partial U}{\partial y}\right] \tag{2.3}$$

This can be integrated from the wall to obtain

$$u_*^2 = < -uv > +\nu\frac{\partial U}{\partial y} \tag{2.4}$$

where u_* is the friction velocity defined as $u_*^2 \equiv \tau_W/\rho$. As the distance from the wall is increased, the viscous stress vanishes and $< -uv > \rightarrow u_*^2$, but only in the infinite Reynolds number limit. At finite Reynolds numbers the outer flow is reached first and the convection terms reduce the Reynolds shear stress before it can reach the limiting value.

It is obvious that the inner profiles must scale with u_* and ν since these are the only parameters in the inner equations and boundary conditions. Hence, there must be a law of the wall (at least for a limited region very close to the wall). This should not be taken to imply, however, that u_*^2 is an independent parameter; it is not. It is uniquely determined by the pressure drop imposed on the pipe, the pipe diameter and the kinematic viscosity.

Because there is no imposed condition on the velocity, except for the no-slip condition at the wall, an outer scaling velocity must be sought from the parameters in the outer equation itself. Since there are only two, $-(1/\rho)dP/dx$, the externally imposed pressure gradient, and R the channel half-width, only a single velocity can be formed; namely,

$$U_o = \left(-\frac{R}{\rho}\frac{dP}{dx}\right)^{1/2} \tag{2.5}$$

Unlike the developing boundary layer, the fully-developed pipe or channel flow is homogeneous in the stream-wise direction, so a straightforward similarity analysis using the x-dependence to establish the scaling parameters is not possible. However, because of this stream-wise homogeneity, there is an exact balance between the wall shear stress acting on the walls, and the net pressure force acting across the flow. For fully-developed channel flow, this equilibrium requires that

$$u_*^2 = -\frac{R}{\rho}\frac{dP}{dx} \tag{2.6}$$

which is just the square of equation 2.5 above; thus, $U_o = u_*$. Therefore, the outer scale velocity is also u_*, and the outer and inner velocity scales are the same. The factor of two which appears in the corresponding pipe flow equilibrium can be ignored in choosing the scale velocity, so the same argument and result apply to it as well.

Thus channel and pipe flows differ from boundary layer flows where asymptotic Reynolds number independence and stream-wise *inhomogeneity* demand that the inner and outer scales for the mean velocity be different (George and Castillo 1997). This consequence of homogeneity on the governing equations themselves is fundamental to understanding the unique nature of pipe and channel flows. Homogeneity is the reason these flows show a logarithmic dependence for the velocity in the overlap region and for the friction law, unlike boundary layers which are characterized by power laws because of their inhomogeneity.

It is obvious that since the length scales governing the inner and outer equations are different, no single scaling law should be able to collapse data for the entire flow. Moreover, since the neglected terms in both the inner and outer equations above depend on the ratio of length scales (v. Tennekes and Lumley 1972), then neither set of scaling parameters will be able to perfectly collapse the data in either region at finite values of $R^+ = Ru_*/\nu$. The Asymptotic Invariance Principle (or AIP, George 1995) states that the appropriate choices for scaling are those which lead to similarity solutions of the inner and outer equations separately in the limit for which those equations themselves are valid, namely $R^+ \to \infty$. Thus the appropriate inner and outer scaled versions of the velocity profile are

$$\frac{U}{u_*} = f_i(y^+, R^+) \tag{2.7}$$

and

$$\frac{U - U_c}{u_*} = f_o(\overline{y}, R^+) \tag{2.8}$$

where the outer velocity has been referenced to the velocity at the centerline, U_c, to avoid the necessity of accounting for viscous effects over the inner layer when the limits are taken later. The outer length scale is some measure of the diameter of the pipe (say the pipe radius) or the width of the channel (say half-width). Both of these will be denoted as R in the remainder of the paper.

Note that the fact that the inner and outer equations are themselves only strictly valid in the limit as $R^+ \to \infty$ means that *no scaling law can perfectly collapse the data except in this limit* since no similarity solutions exist except here. In fact, both equations 2.7 and 2.8 describe the *entire* velocity profile as long as $R^+ = u_*R/\nu$, the ratio of outer to inner length scales, is retained. This is because they represent the same solutions to the complete governing equations for a given R^+, but have simply been scaled differently.

Properly scaled profiles should by the Asymptotic Invariance Principle (AIP, George 1995) become asymptotically independent of R^+ in the limit of infinite Reynolds number; i.e.,

$$\lim f_i(y^+, R^+) \to f_{i\infty}(y^+)$$
$$\lim f_o(\overline{y}, R^+) \to f_{o\infty}(\overline{y})$$

as $R^+ \to \infty$. In fact, these limiting profiles should be solutions to the inner and outer equations respectively (i.e., equations 2.3 and 2.2), which are themselves valid only in the infinite Reynolds number limit.

Figures 1 and 2 show the mean velocity profile data from the Princeton superpipe experiment (Zagarola 1996, see also Zagarola and Smits 1996) in both inner and outer variables. Note the excellent collapse very close to the wall for $y^+ < 100$ in inner variables, and over the core region for $\overline{y} > 0.3$. Note also that the region of approximate collapse in inner variables (Figure 1) increases from the wall with increasing Reynolds number, as does the inward extent of the outer variable collapse (Figure 2). Finally note that the inner scaling does not collapse the data at all where the outer scaling collapses it best, and vice versa. Both the region of approximate collapse and the region of no collapse at all are manifestations of the dependence of the scaled profiles on R^+ as argued above.

Unlike boundary layer experiments, the wall shear stress for the fully-developed pipe flow can be determined from the pressure drop down the pipe alone, entirely independent from the velocity profile measurements. The direct determination of the shear stress from the pressure drop without choosing it to collapse a 'log' layer which can only be assumed to collapse (the so-called Clauser method) is especially important since, as noted above

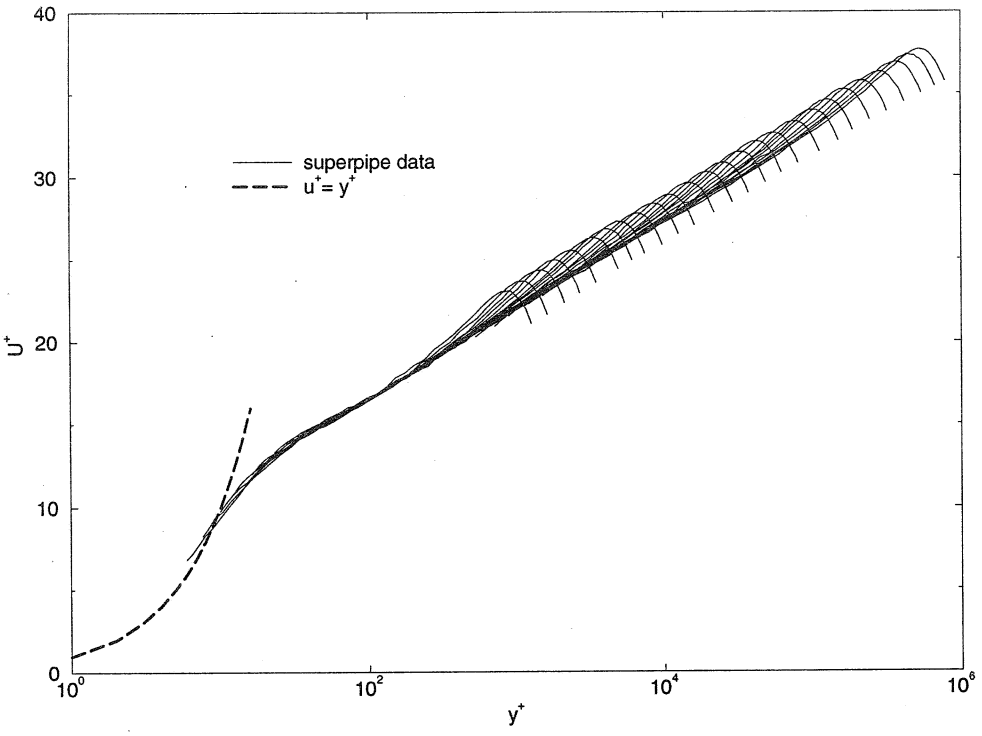

FIGURE 1. Velocity profiles in inner variables

there is evidence of a lack of complete collapse of the data in Figure 1 *outside* of $y^+ = 100$, especially for the lowest Reynolds numbers. The lack of collapse is even more apparent for the outer scaling in Figure 2 *inside* of $\overline{y} \approx 0.3$ which includes all of the overlap region discussed below.

3. The Overlap Layer: An Application of Near-Asymptotics

It is obvious that since the outer and inner profiles scale differently and the ratio of length scales is in fact the Reynolds number, then the region between the two similarity regimes cannot be Reynolds number independent, except possibly in the limit of infinite Reynolds number. The actual mean velocity profile at any finite Reynolds number, however, is the average of the instantaneous solutions to the Navier-Stokes equations and boundary conditions. And this profile, whether determined from a real flow by measurement, a DNS simulation, or not at all, exists, at least in principle, and is valid everywhere *regardless of how it is scaled.* Therefore both scaled forms of this solution, $f_i(y^+, R^+)$ and $f_o(\overline{y}, R^+)$ (equations 2.7 and 2.8 respectively), represent the velocity everywhere, at least as long as the Reynolds number is finite. In fact, the parameter R^+ uniquely labels the fanning out of the inner scaled profiles in the outer region and the outer scaled profiles near the wall in Figures 1 and 2.

Thus, f_i and f_o are quite unlike their limiting forms, $f_{i\infty}$ and $f_{o\infty}$, which are only infinite Reynolds number solutions for the inner and outer equations respectively. If f_i and f_o are considered instead of $f_{i\infty}$ and $f_{o\infty}$ (as is usually done), the problem of

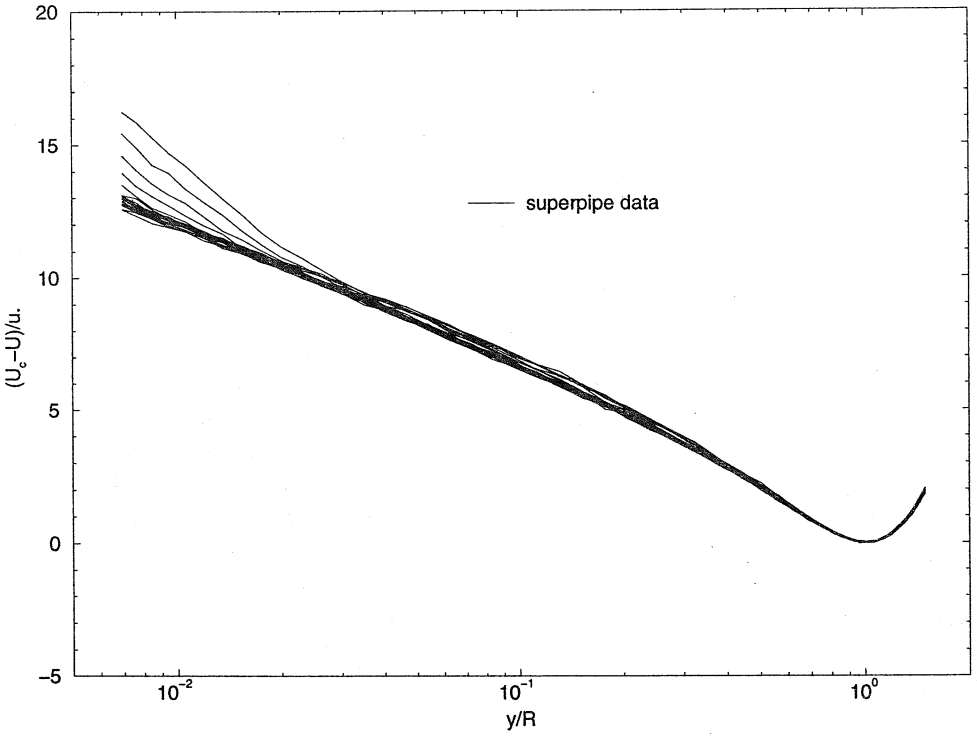

FIGURE 2. Velocity profiles in outer variables

determining whether an overlap region exists is quite different from the usual asymptotic matching where infinite Reynolds number inner and outer solutions are extended and matched in an overlap region if one exists. Therefore, the objective here is *not* to see if f_i and f_o overlap and match them if they do. Rather, it is rather to determine *whether the fact that these scaled finite Reynolds number solutions (to the whole flow) degenerate at infinite Reynolds number in different ways* can be used to determine their functional forms in the common region they describe in the limit. The methodology, termed *Near-Asymptotics* was first utilized by George 1995 (see also George and Castillo 1997), and is necessary because the traditional approach cannot account for the possibility of the matching parameter tending to zero, as might be the case. It also makes the results easier to compare to experiments since most are carried out far from asymptotic conditions.

The fact that analytical forms for these Reynolds number dependent solutions are not available, and they are only known *in principal* turns out not to be a significant handicap. There are several pieces of information about the two profiles which can be utilized without further assumptions. They are:

- First, since both inner and outer forms of the velocity profile must describe the flow everywhere as long as the ratio of length scales, $R^+ = R/\eta$, is finite, it follows from equations 2.7 and 2.8 that

$$\frac{1}{g(R^+)} + f_o(\overline{y}, R^+) = f_i(y^+, R^+) \tag{3.1}$$

where $g(R^+)$ is defined by

$$g(R^+) \equiv u_*/U_e \tag{3.2}$$

• Second, for finite values of R^+, the velocity derivatives from both inner and outer forms of the velocity must also be the same everywhere. It is easy to show that this implies that

$$\overline{y}\frac{\partial f_o}{\partial \overline{y}} = y^+\frac{\partial f_i}{\partial y^+} \tag{3.3}$$

for all values of R^+ and y.

• Third, as noted above, in the limit both f_o and f_i must become asymptotically independent of R^+; i.e., $f_o(\overline{y}, R^+) \to f_{o\infty}(\overline{y})$ and $f_i(y^+, R^+) \to f_{i\infty}(y^+)$ as $R^+ \to \infty$.

Now the problem is that *in the limit* as $R^+ \to \infty$, the outer form fails to account for the behavior close to the wall while the inner fails to describe the behavior away from it. The question then is: In this limit (as well as for all finite values approaching it) does there exist an "overlap" region where equation 3.1 is still valid? (Note that boundary layer flows are quite different from pipe and channel flows since the overlap layer in the latter remains at fixed distance from the wall for all x because of the stream-wise homogeneity, as long as the external parameters — like geometry and Reynolds number — are fixed, while in the former it moves away from the wall with increasing x.)

The question of whether there is a common region of validity can be investigated by examining how rapidly f_o and f_i are changing with R^+. The relative variation of f_i and f_o with Reynolds number can be related to their Taylor expansions about a fixed value of R^+; i.e.,

$$\frac{f_i(y^+; R^+ + \Delta R^+) - f_i(y^+; R^+)}{\Delta R^+ f_i(y^+, R^+)} \approx \frac{1}{f_i(y^+, R^+)}\frac{\partial f_i(y^+; R^+)}{\partial R^+}\Big|_{y^+} \equiv S_i(R^+, y^+) \tag{3.4}$$

and

$$\frac{f_o(\overline{y}; R^+ + \Delta R^+) - f_o(\overline{y}; R^+)}{\Delta R^+ f_o(\overline{y}, R^+)} \approx \frac{1}{f_o(\overline{y}, R^+)}\frac{\partial f_o(\overline{y}; R^+)}{\partial R^+}\Big|_{\overline{y}} \equiv S_o(R^+, \overline{y}) \tag{3.5}$$

Thus S_i and S_o are measures of the Reynolds number dependence of f_i and f_o respectively. Both vanish identically in the limit as $R^+ \to \infty$. If ${y^+}_{max}$ denotes a location where outer flow effects begin to be strongly felt on the inner scaled profile, then for $y^+ < {y^+}_{max}$, S_i should be much less than unity (or else the inner scaling is not very useful). Similarly, if $\overline{y}_{min}$ measures the location where viscous effects begin to be strongly felt (e.g., as the linear velocity region near the wall is approached), then S_o should be small for $\overline{y} > \overline{y}_{min}$. Obviously either S_i or S_o should increase as these limits are approached. Outside these limits, one or the other should increase dramatically.

The quantities S_i and S_o can, in fact, be used to provide a formal definition of an "overlap" region where both scaling laws are valid. Since S_i will increase drastically for large values of y for given R^+, and S_o will increase for small values of y, an "overlap" region exists only if there exists a region for which both S_i and S_o remain small simultaneously. In the following paragraphs, this condition will be used in conjunction with equation 3.1 to derive the functional form of the velocity in the overlap region *at finite Reynolds number*, hence the term 'Near-Asymptotics'.

Because of the movement of the overlap region toward the wall with increasing R^+, it is convenient and necessary to introduce an intermediate variable $\tilde{y}$ which can be fixed in the overlap region all the way to the limit, regardless of what is happening in physical space (v. Cole and Kevorkian 1981). A definition of $\tilde{y}$ which accomplishes this is given

by

$$\tilde{y} = y^+ {R^+}^{-n} \tag{3.6}$$

or

$$y^+ = \tilde{y} {R^+}^{n} \tag{3.7}$$

Since $R^+ = y^+/\overline{y}$, it follows that

$$\overline{y} = \tilde{y} {R^+}^{n-1} \tag{3.8}$$

For all values of n satisfying $0 < n < 1$, $\tilde{y}$ can remain fixed in the limit as $R^+ \to \infty$ while $\overline{y} \to 0$ and $y^+ \to \infty$. Substituting these into equation 3.1 yields the matching condition on the velocity in terms of the intermediate variable as

$$\frac{1}{g(R^+)} + f_o({R^+}^{n-1}\tilde{y}, R^+) = f_i({R^+}^{n}\tilde{y}, R^+) \tag{3.9}$$

Now equation 3.9 can be differentiated with respect to R^+ *for fixed* $\tilde{y}$ to yield equations which explicitly include S_i and S_o. The result after some manipulation is

$$\overline{y}\left(\frac{\partial f_o}{\partial \overline{y}}\right)_{R^+} = \frac{1}{\kappa} - R^+[S_i(y^+, R^+)f_i(y^+, R^+) - S_o(\overline{y}, R^+)f_o(\overline{y}, R^+)] \tag{3.10}$$

where

$$\frac{1}{\kappa(R^+)} \equiv -\frac{R^+}{g^2}\frac{dg}{dR^+} = \frac{d(1/g)}{d\ln R^+} \tag{3.11}$$

The first term on the right hand side of equation 3.10 is at most a function of R^+ alone, while the second term contains all of the residual y-dependence. Note that the factor of R^+ could have been absorbed into the definitions of S_i and S_o by simply defining them as the logarithmic derivatives of the inner and outer scaled profiles.

Now it is clear that if both

$$R^+|S_o|f_o << 1/\kappa \tag{3.12}$$

and

$$R^+|S_i|f_i << 1/\kappa \tag{3.13}$$

then the first term on the right-hand side of equation 3.10 dominates. If $1/\kappa \to 0$, then the inequalities are still satisfied as long as the left hand side does so more rapidly than $1/\kappa$. Note that a much weaker condition can be applied which yields the same result; namely that both inner and outer scaled profiles have the same dependence on R^+; i.e., $S_i f_i = S_o f_o$ in the overlap range so $1/\kappa$ is the only term remaining. If these inequalities are satisfied over some range in y, then to leading order, equation 3.10 can be written as

$$\overline{y}\frac{\partial f_o}{\partial \overline{y}} = \frac{1}{\kappa} \tag{3.14}$$

The solution to equation 3.14 could be denoted as $f_o^{(1)}$ since it represents a first order approximation to f_o. It is *not*, however, simply the same as $f_{o\infty}$ because of the R^+ dependence of $1/\kappa$, but reduces to it in the limit. Thus, by regrouping into the leading term all of the y-independent contributions, the method applied here has yielded a more general result than the customary expansion about infinite Reynolds number. (It is also easy to see why the usual matching of infinite Reynolds number inner and outer solutions will not work if the limiting value of $1/\kappa$ is zero, which can not yet be ruled out.)

From equations 3.3 and 3.14, it follows that

$$y^+ \frac{\partial f_i}{\partial y^+} = \frac{1}{\kappa} \tag{3.15}$$

Equations 3.14 and 3.15 must be independent of the origin for y; hence they must be invariant to transformations of the forms $\overline{y} \rightarrow \overline{y} + \overline{a}$ and $y^+ \rightarrow y^+ + a^+$ respectively, where a is at most a function of the Reynolds number. Therefore the most general overlap solutions are of the form,

$$\frac{U - U_c}{u_*} = f_o(\overline{y}, R^+) = \frac{1}{\kappa(R^+)} ln[\overline{y} + \overline{a}(R^+)] + B_o(R^+) \tag{3.16}$$

and

$$\frac{U}{u_*} = f_i(y^+, R^+) = \frac{1}{\kappa(R^+)} ln[y^+ + a^+(R^+)] + B_i(R^+) \tag{3.17}$$

The superscript '(1)' has been dropped; however it is these first order solutions that are being referred to unless otherwise stated. Thus the velocity profiles in the overlap region are logarithmic, but with parameters which are in general Reynolds number dependent. Note that the particular form of the solution $\ln(y+a)$ has been also identified by Oberlack (1996) from a Lie group analysis of the equations governing homogeneous shear flows. It will be argued in Section 7 below that a^+ is closely related to the mesolayer, just as it is for the boundary layer (George and Castillo 1997). The data will be found to be consistent with $a^+ \approx -8$.

An interesting feature of these first order solutions is that the inequalities given by equations 3.12 and 3.13 determine the limits of validity of both equations 3.14 and 3.15 since either S_o or S_i will be large outside the overlap region. Clearly the extent of this region will increase as the Reynolds number (or R^+) increases.

The parameters $1/\kappa$, B_i and B_o must be asymptotically constant since they occur in solutions to equations which are themselves themselves Reynolds number independent in the limit (the AIP). Moreover, the limiting values, κ_∞, $B_{i\infty}$, and $B_{o\infty}$ cannot all be zero, or else the solutions themselves are trivial. In fact, in the limit of infinite Reynolds number the energy balance in the overlap range reduces to production equals dissipation; i.e., $\epsilon^+ = P^+$. In section 7 below this will be shown to imply that

$$\epsilon \rightarrow \frac{du^+}{dy^+} = \frac{1}{\kappa(y^+ + a^+)} \tag{3.18}$$

Since the *local* energy dissipation rate must be finite and non-zero (Frisch 1995), it follows that $1/\kappa_\infty$ must be finite and non-zero. It will be shown below that these conditions severely restrict the possible Reynolds number dependencies for the parameters κ, B_i and B_o. (It is interesting to note that the same physical constraint on the boundary layers results requires that the power exponent, γ be asymptotically finite and non-zero in the limit of infinite Reynolds number.)

The relation between u_* and U_c follows immediately from equation 3.1; i.e.,

$$\frac{U_c}{u_*} = \frac{1}{g(R^+)} = \frac{1}{\kappa(R^+)} ln R^+ + [B_i(R^+) - B_o(R^+)] \tag{3.19}$$

Thus the friction law is entirely determined by the velocity parameters for the overlap region. However, equation 3.11 must also be satisfied. Substituting equation 3.19 into equation 3.11 implies that κ, B_i, and B_o are constrained by

$$\ln R^+ \frac{d(1/\kappa)}{d \ln R^+} = -\frac{d(B_i - B_o)}{d \ln R^+} \tag{3.20}$$

But this is exactly the criterion for the neglected terms in equation 3.10 to vanish identically (i.e., $S_i f_i - S_o f_o \equiv 0$). Therefore the solution represented by equations 3.16 to 3.20 is, indeed, the first order solution for the velocity profile in the overlap layer at *finite*, but large, Reynolds number. Clearly when y^+ is too big or $\overline{y}$ is too small for a given value of R^+, the inequalities of equation 3.12 and 3.13 cannot be satisfied. Since all the derivatives with respect to R^+ must vanish as $R^+ \to \infty$ (the AIP), the outer range of the inner overlap solution is unbounded in the limit, while the inner range of the outer is bounded only by $\overline{y} = -\overline{a}$.

Equation 3.20 is invariant to transformations of the form $R^+ \to D_s R^+$ where D_s is a scale factor which insures that the functional dependence is independent of the particular choice of the outer length scale (e.g., diameter versus radius). Thus the velocity profile in the overlap layer is logarithmic, *but* with parameters which depend on the Reynolds number, $D_s R^+$. The functions $\kappa(D_s R^+)$, $B_i(D_s R^+)$ and $B_o(D_s R^+)$ must be determined either empirically or from a closure model for the turbulence. Regardless of how they are determined, the results must be consistent with equation 3.20. Obviously the appropriate form of the independent variable is $\ln D_s R^+$, and not just R^+ alone.

4. A Solution for the Reynolds Number Dependence

It is convenient to transform equation 3.20 using

$$H(D_s R^+) \equiv \left(\frac{1}{\kappa} - \frac{1}{\kappa_\infty}\right) \ln D_s R^+ + (B_i - B_o) \tag{4.1}$$

where $H = H(D_s R^+)$ remains to be determined. It is easy to show that if $H(D_s R^+)$ satisfies

$$\frac{1}{\kappa} - \frac{1}{\kappa_\infty} = \frac{dH}{d \ln D_s R^+} \tag{4.2}$$

then equation 3.20 is satisfied. It follows immediately that

$$\frac{1}{g} = \frac{U_c}{u_*} = \frac{1}{\kappa_\infty} \ln D_s R^+ + H(D_s R^+) \tag{4.3}$$

Thus the Reynolds number dependence of the single function $H(DR_s^+)$ determines that of κ, $B_i - B_o$ and g.

The conditions that both $B_{i\infty}$ and $B_{o\infty}$ be finite and non-zero require that:

Either

- B_i, B_o and κ remain constant always;

or

- (i) $1/\kappa \to 1/\kappa_\infty$ faster than $1/\ln D_s R^+$, and
- (ii) $H(D_s R^+) \to H_\infty = constant$.

Obviously from equation 4.1,

$$H_\infty = B_{i\infty} - B_{o\infty} \tag{4.4}$$

An empirical choice for $H(D_s R^+) - H_\infty$ satisfying these conditions is suggested by the boundary layer analysis of George and Castillo (1997); it is,

$$H(D_s R^+) - H_\infty = \frac{A}{[\ln D_s R^+]^\alpha} \tag{4.5}$$

Note that conditions (i) and (ii) above imply that $\alpha > 0$.

Using this in equation 4.3 yields

$$\frac{U_c}{u_*} = \frac{1}{\kappa_\infty} \ln D_s R^+ + [B_{i\infty} - B_{o\infty}] + \frac{A}{[\ln D_s R^+]^\alpha} \tag{4.6}$$

As $R^+ \to \infty$ this reduces to the classical solution of Millikan 1938. This is comforting since Millikan's analysis is an infinite Reynolds number analysis of inner and outer profiles scaled in the same way. (Note that this was *not* true for the boundary layer: The Clauser/Millikan analysis *assumed* the same scaling laws applied as for the pipe. George/Castillo argued from the Reynolds-averaged equations that they had to be different, hence the different conclusions.)

The Reynolds number variation of $1/\kappa$ and $B_i - B_o$ can be immediately obtained from equations 4.1, 4.2 and 4.5 as

$$\frac{1}{\kappa} - \frac{1}{\kappa_\infty} = -\frac{\alpha A}{(\ln D_s R^+)^{1+\alpha}} \tag{4.7}$$

and

$$(B_i - B_o) - (B_{i\infty} - B_{o\infty}) = \frac{(1+\alpha)A}{(\ln D_s R^+)^\alpha} \tag{4.8}$$

Figures 3a and 3b show the friction data of the superpipe experiment of Zagarola and Smits (1996). As the investigators themselves have pointed out, careful scrutiny reveals that the data do not fall on a straight line, so a simple logarithmic friction law with constant coefficients does not describe all the data *to within the accuracy of the data itself.* In particular, a log which attempts to fit all of the data dips away from it in the middle range. On the other hand, a log which fits the high Reynolds number range does not fit the low, or vice versa. Figure 3b shows two curves: The first represents a regression fit of equation 4.6 (also shown on Figure 3a), while the second shows only the asymptotic log form of equation 4.6. The former provides an excellent fit to the data for *all* Reynolds numbers and asymptotes exactly to the latter, but only at much higher Reynolds numbers. The differences although slight are very important since they entirely determine (or reflect) the Reynolds number dependence of the parameters $1/\kappa$, B_i and B_o. The latter will be seen later to be especially sensitive to this dependence. Clearly the proposed form of H captures the residual Reynolds number dependence, while simply using constant coefficients does not.

The values obtained for the asymptotic friction law parameters using optimization techniques are $\kappa_\infty = 0.447$, $B_{i\infty} - B_{o\infty} = 8.45$, while those describing the Reynolds number dependence are $A = -0.668$ and $\alpha = 0.441$. The same optimization techniques showed no advantage to using values of the parameter D_s different from unity, hence $D_s = 1$ to within experimental error. Note that the values of $B_{i\infty}$ and $B_{o\infty}$ cannot be determined individually from the friction data, only their difference. Nominal values for κ and $B_i - B_o$ are approximately 0.445 and 8.20 respectively, the former varying by less than 0.5% and the latter by only one percent over the entire range of the data. These values differ only slightly from the values determined by Zagarola (1996) (0.44 and 7.8 respectively) using the velocity profiles alone and assuming that the asymptotic state had been reached. In fact it will be shown later from the velocity profiles that B_i is independent of Reynolds number and equal to 6.5. Thus only B_o significantly changes with the Reynolds number and then only by about 5% over the range of the data, but even this variation will be seen to be quite important for the outer profile. Note that the friction law is independent of the parameter a.

All the parameters are remarkably independent of the particular range of data utilized. For example, of the 26 different Reynolds numbers available, the highest 15 Reynolds

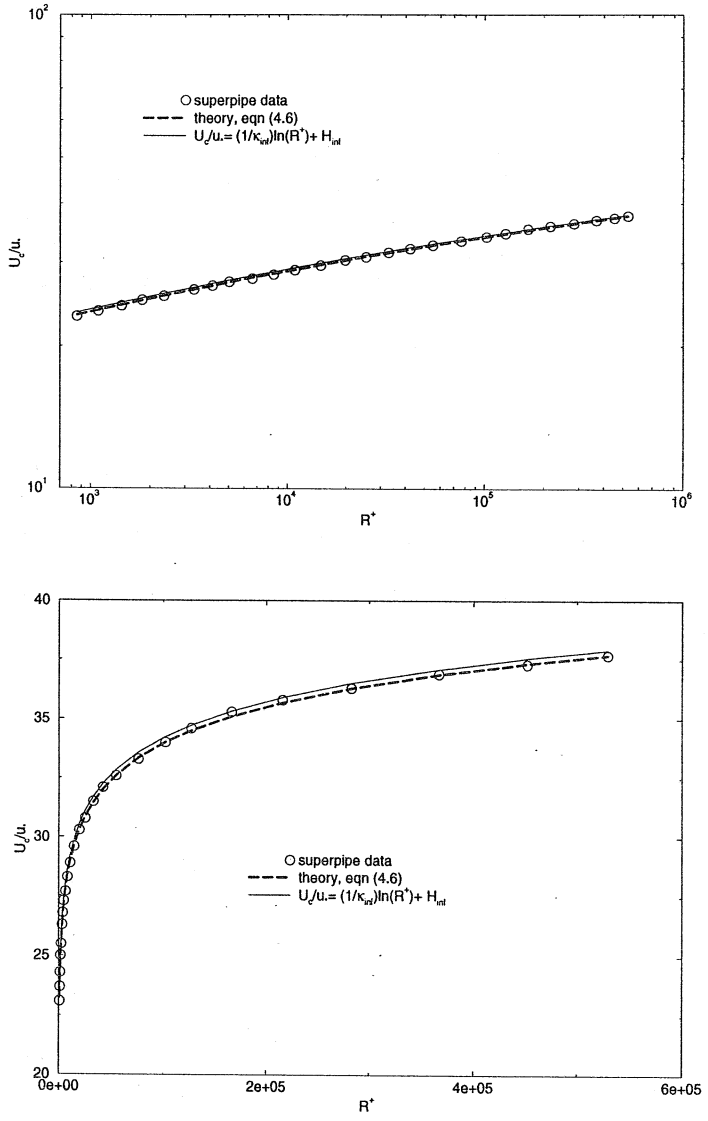

FIGURE 3. Variation of U_c/u_* with $R^+ = Ru_*/\nu$

numbers could be dropped before even changing the second digit of the values of the parameters cited above. This suggests strongly, contrary to the suggestion of Barenblatt et al. 1997, that the superpipe data are in fact a smooth curve, uncontaminated by roughness. If the analysis developed herein is correct, then the reason these authors had a problem with the superpipe data is obvious: the data vary logarithmically as *derived* here, and not according to their *conjectured* power law.

For the boundary layer the friction data are not as reliable as those reported here, so the functional form of $h(\delta^+)$ had to be inferred after a variety of attempts to describe the variation of the exponent in a power law description of the velocity profile in the overlap region. Interestingly, the value for α obtained here is almost exactly the value

obtained for the boundary layer data (0.46 versus 0.44). Even more intriguing is that both of these are nearly equal to the values found for κ_∞ and $1/(\gamma_\infty C_{i\infty})$. It is not yet clear whether there is physical significance to this, or whether it is just coincidence.

5. Single-point Second-order Turbulence Quantities.

Unlike the boundary layer where the continued downstream evolution imposes certain similarity constraints, for pipe and channel flows there is only a single velocity scale so all quantities must scale with it. An immediate consequence of this is that all quantities scaling with the velocity only will have logarithmic profiles in the overlap region. (It is straightforward to show this by exactly the procedures applied above to the velocity.)

For example, in inner variables, the Reynolds stress profiles are given by

$$< -u_m u_n >^+ = \frac{< -u_m u_n >}{u_*^2} = A_{imn}(R^+)\ln(y^+ + a^+) + B_{imn}(R^+) \qquad (5.1)$$

As for the velocity, the parmeters A_{imn} and B_{imn} are functions of the Reynolds number and only asymptotically constant. Note that the offset a^+ has been assumed to be the same as for the velocity, although this needs to be subjected to experimental verification.

The Reynolds shear stress is particularly interesting since for it more information can be obtained from the mean momentum equation. In the overlap region in the limit as $R^+ \to \infty$, both equations 2.2 and 2.3 reduce to

$$0 = \frac{\partial < -uv >}{\partial y} \qquad (5.2)$$

or in inner variables,

$$0 = \frac{\partial < -uv >^+}{\partial y^+} \qquad (5.3)$$

It follows from substituting the 1, 2-component of equation 5.1 that

$$0 = \frac{A_{i12}}{y^+ + a^+} \qquad (5.4)$$

It is immediately clear that equation 5.3 can be satisfied only if $A_{i12} \to 0$ as $R^+ \to \infty$. A similar argument for the outer profile implies $A_{o12} \to 0$. Thus to leading order, the Reynolds shear stress profile in the overlap region is independent of y; however, the remaining parameters B_{i12} and B_{o12} are only asymptotically constant. From equation 2.4 it is clear that $B_{i12} \to 1$, but only in the limit. Since $< -uv > \to u_*^2$ is also the inner boundary condition on equation 2.2, $B_{o12} \to 1$ in the limit also.

Another quantity of particular interest is the rate of dissipation of turbulence energy per unit mass, ϵ. In the inner part of the flow, the appropriate dissipation scale can easily be shown on dimensional grounds to be u_*^4/ν since there are no other possibilities. In the outer layer in the limit of infinite Reynolds number, the dissipation is effectively inviscid (as discussed in Section 6 below) so it must scale as u_*^3/R. (Note that this only means that the profiles scaled as $\epsilon\nu/u_*^4$ versus y^+ and $\epsilon R/u_*^3$ versus $\overline{y}$ will collapse in the limit of infinite Reynolds number in the inner and outer regions respectively.) It is easy to show by the methodology applied to the velocity and Reynolds stresses above that the dissipation profile in the overlap region is given by a *power law* with an exponent of -1. Thus

$$\epsilon^+ = \frac{\epsilon\nu}{u_*^4} = \frac{E_i(R^+)}{y^+ + a^+} \qquad (5.5)$$

and

$$\overline{\epsilon} = \frac{\epsilon R}{u_*^3} = \frac{E_o(R^+)}{\overline{y} + \overline{a}} \tag{5.6}$$

where both E_o and E_i are asymptotically constant. It has again been assumed that the origin shift a is the same as for the velocity. For the dissipation, this can be justified using the production equals dissipation limit as shown in the Section 7.

6. The Effect of Reynolds Number on the Overlap Range

The parameters established for the friction law above will be used below to calculate the values of κ, B_i and B_o for each Reynolds number of the superpipe data. Only either of the B's need be established from the experiments since their difference is known from equation 4.1. Before carrying out a detailed comparison with the velocity data, however, it is is useful to first consider exactly which region of the flow is being described by the overlap profiles. Also of interest is the question of how large the Reynolds number must be before the flow begins to show the characteristics of the asymptotic state.

The overlap layer identified in the preceding sections can be related directly to the averaged equations for the mean flow and the Reynolds stresses. From about $y^+ > 30$ out to about the center of the flow, the averaged momentum equation is given approximately by

$$0 = -\frac{1}{\rho}\frac{dP}{dx} + \frac{\partial < -uv >}{\partial y} \tag{6.1}$$

It has no explicit Reynolds number dependence; and the Reynolds shear stress drops linearly all the way to the center of the flow (v. Perry and Abell 1975). Inside about $\overline{y} = 0.1$ and outside of $y^+ = 30$, however, the Reynolds shear stress is very nearly constant. In fact, at infinite Reynolds number the pressure gradient term vanishes identically in the constant Reynolds shear stress region and the mean momentum equation reduces to

$$0 = \frac{\partial < -uv >}{\partial y} \tag{6.2}$$

At finite (but large) Reynolds numbers this region is similar to the developing boundary layer where the Reynolds stress is effectively constant. Obviously *the overlap region corresponds to this constant Reynolds shear stress layer* since the Reynolds shear stress gradient is the common term to both inner and outer momentum equations. Note that many low Reynolds number experiments do not have a region where the Reynolds stress is even approximately constant because the pressure gradient term is not truly negligible. Hence it is unreasonable to expect such experimental profiles to display any of the characteristics of the overlap described above, except possibly in combination with the characteristics of the other regions (e.g., through a composite solution).

Even when there is a region of reasonably constant Reynolds stress, however, this is not the entire story because of the Reynolds number dependence of $< -uv >$ itself. And it is this weak Reynolds number dependence which is the reason that κ, B_i, and B_o are only asymptotically constant. The origin of this weak Reynolds number dependence (which is well-known to turbulence modelers) can be seen by considering the Reynolds transport equations. For the same region, $y^+ > 30$, the viscous diffusion terms are negligible (as in the mean momentum equation), so the Reynolds shear stress equations

reduce approximately to (Tennekes and Lumley 1972),

$$0 = -(< p\frac{\partial u_i}{\partial x_k} > + < p\frac{\partial u_k}{\partial x_i} >) - \left[< u_i u_2 > \frac{\partial U_k}{\partial x_2} + < u_k u_2 > \frac{\partial U_i}{\partial x_2} \right] - \frac{\partial < u_i u_k u_2 >}{\partial x_2} - \epsilon_{ik} \tag{6.3}$$

where $U_i = U\delta_{i1}$. Thus viscosity does not appear directly in any of the single point equations governing the overlap region, nor does it appear in those governing the outer layer.

In spite of the above, however, viscosity can be shown to play a crucial role in at least a portion of the constant stress layer, even at infinite Reynolds number. The reason is that the *length scales* at which the dissipation, ϵ_{ik}, actually takes place depend on the *local* turbulence Reynolds number, $R_t = q^4/\nu\epsilon$. For $R_t > 5000$ approximately, the energy dissipation is nearly completely determined by the large energetic scales of motion. These scales are effectively inviscid, but control the energy transfer through non-linear interactions (the energy cascade) to the much smaller viscous scales where the actual dissipation occurs (v. Tennekes and Lumley 1972). When this is the case, the dissipation is nearly isotropic so $\epsilon_{ik} \approx 2\epsilon\delta_{ik}$. Moreover, ϵ can be approximated by the infinite Reynolds number relation: $\epsilon \sim q^3/L$ where L is a scale characteristic of the energy-containing eddies. The coefficient has a weak Reynolds number dependence, but is asymptotically constant. Thus, the Reynolds stress equations themselves are effectively inviscid, but only exactly so in the limit. Note that in this limit the Reynolds shear stress has no dissipation at all, i.e., $\epsilon_{12} = 0$.

At very low turbulence Reynolds number, however, the dissipative and energy-containing ranges nearly overlap, and so the latter (which also produce the Reynolds shear stress) feels directly the influence of viscosity. In this limit, the energy and dissipative scales are about the same, so the dissipation is more reasonably estimated by $\epsilon \sim \nu q^2/L^2$, where the constant of proportionality is of order 10. The dissipation tensor, ϵ_{ik} is anisotropic and ϵ_{12}, in particular, is non-zero. (Hanjalic and Launder 1974, for example, take $\epsilon_{12} = (- < u_1 u_2 > \epsilon/q^2)$.)

For turbulence Reynolds numbers between these two limits, the dissipation will show characteristics of both limits, gradually making a transition from $\epsilon \sim \nu q^2/L^2$ to $\epsilon \sim q^3/L$ as R_t increases. Thus the Reynolds stresses themselves will feel directly this, and will show a strong Reynolds number dependence. Obviously, in order to establish when (if at all) parts of the flow become Reynolds number independent, it is necessary to determine how the local turbulence Reynolds number varies across the flow.

Over the outer part of the pipe (which is most of it), $L \approx R/2$ and $q \approx 3u_*$. So when $R^+ > 3,000$, the dissipation in the outer flow is effectively inviscid. Above this value the mean and turbulence quantities in the core region of the flow should show little Reynolds number dependence, This is indeed the case as illustrated by Figure 2. The outer region can, of course, not be entirely Reynolds number independent, except in the limit, and this residual dependence manifests itself in the overlap layer in the slow variations of κ and B_o, for example.

The near wall region is considerably more interesting since in it the scales governing the energy-containing eddies are constrained by the proximity of the wall. Hence, the turbulence Reynolds number, R_t, depends on the distance from the wall, y. In fact, $R_t \sim y^+$ with a coefficient of about 18 (Gibson 1997); so, in effect, y^+ is the turbulence Reynolds number. Because of this, two things are immediately obvious:

- First, as the Reynolds number increases more and more of the pipe (in outer variables) will become effectively inviscid and will be governed by the inviscid dissipation relation. And correspondingly, the properly scaled mean and turbulence quantities in at

least the outer part of the overlap layer (say, an INERTIAL SUBLAYER) will become Reynolds number independent, albeit very slowly. Clearly these limiting values cannot be reached until the layer is governed by the infinite Reynolds number dissipation relation and its coefficient has reached the limiting value. Obviously this can happen only when there is a substantial inertial sublayer satisfying $y^+ > 300$ (approximately) and for which the mean pressure-gradient term is negligible, typically $\overline{y} < 0.1$. Thus the asymptotic limits are realized only when $300\nu/u_* << 0.1R$ or $R^+ >> 3000$. Therefore below $R^+ = 30,000$ approximately, even this inertial sublayer should display a Reynolds number dependence, not only in κ, B_o, and B_i, but correspondingly in the behavior of $< u^2 >$, $< uv >$, etc. Note that the lower limit of this inertial sublayer also corresponds (for the same reasons) to the place where a $k^{-5/3}$-region should begin to be observed in the energy spectra.

• Second, at the bottom of the overlap region (or the constant Reynolds shear stress layer) there will always be a *MESOLAYER* † below about $y^+ \approx 300$ in which the dissipation can *never* assume the character of a high Reynolds number flow, no matter how high the Reynolds number becomes. This is because the dissipation (and Reynolds stress as well) can never become independent of viscosity in this region. Even though the single-point Reynolds-averaged equations are all inviscid above $y^+ \approx 30$, the multipoint equations are not! This fact is well-known to turbulence modelers (v. Hanjalic and Launder 1974), but the consequences for similarity theory and asymptotic analyses do not seem to have been noticed previously. It is particularly important for experimentalists who have routinely tried to apply asymptotic formulas to data from to this region, wrongly believing the mesolayer to be the overlap region.

Thus, as illustrated in Figure 4, the constant stress layer is really two separate regions, each having their own unique character: the *constant Reynolds shear stress (or overlap) region* and *the viscous sublayer* where the viscous stress is also important. Each of these has two subregions. The overlap region consists of an *inertial sublayer* ($y^+ > 300$, $\overline{y} < 0.1$) which is nearly inviscid, and a *mesolayer* ($30 < y^+ < 300$) in which the viscous stresses are negligible, but in which viscosity acts directly on the turbulence scales producing the Reynolds stresses. The viscous sublayer is comprised of a buffer layer ($3 < y^+ < 30$) where the Reynolds stress and viscous stress both act directly on the mean flow; and the linear sublayer near the wall ($y^+ < 3$) where the viscous stresses dominate. And of these four regions, the inertial sublayer will be the *last* to appear as the Reynolds number is increased. *Thus, the overlap layer itself will be most difficult to identify at the modest Reynolds numbers of most laboratory experiments.* unless the properties of the mesolayer are known. In the next section it will be argued that in fact, it is the offset parameter a^+ which accounts for it. Thus the inertial sublayer can readily be identified as the region for which $y^+ >> |a^+|$ and the velocity profile in it is primarily a log profile in y alone, the contribution of the offset being negligible; i.e., $\ln(y+a) \approx \ln y$. Thus a log layer (in y), to the extent that it exists at all, should be sought only outside of $y^+ = 300$. Obviously *attempts to identify logarithmic behavior inside* $y^+ = 300$ *from straight lines on semi-log plots of* u^+ *versus* y^+ *make little sense* if the theory presented herein is correct because of the presence of a. They will, of course, always succeed as a local approximation, but the coefficients so determined will be incapable of extension to

† This appropriates a term from Long 1976 (see also Long and Chen 1982) who argued strongly for its existence, but from entirely different physical and scaling arguments which we find untenable. Nonetheless, despite the skepticism which greeted his ideas, Long's instincts were correct.

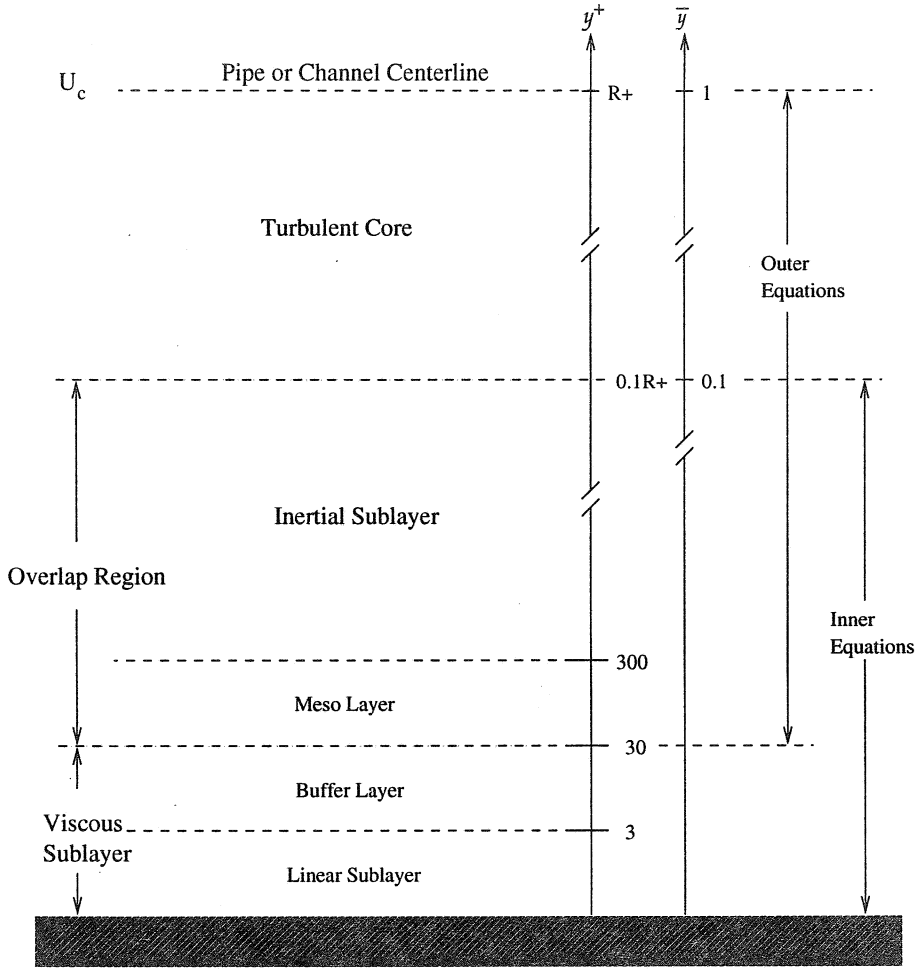

FIGURE 4. Schematic showing various regions and layers of pipe and channel flows

higher values of y^+ as the Reynolds number is increased. And this is indeed the history of attempts to identify the log layer and its parameters from such data.

7. A Mesolayer Interpretation of a^+

The overlap solution of equation 3.17 can be expanded for values of $y^+ >> |a^+|$ to obtain

$$\frac{U}{u_*} = \frac{U}{u_*} = f_i(y^+, R^+) = \frac{1}{\kappa}\{[lny^+ + \kappa B_i] + \frac{a^+}{y^+} - \frac{1}{2}\frac{a^{+2}}{y^{+2}} + \frac{1}{3}\frac{a^{+3}}{y^{+3}} + \ldots\} \tag{7.1}$$

For $y^+ >> |(2a^+|$, this can be approximated by the first three terms as

$$\frac{U}{u_*} = \frac{1}{\kappa}\ln y^+ + B_i + \frac{a^+}{\kappa y^+} \tag{7.2}$$

An equivalent expansion in outer variables is given by

$$\frac{U - U_c}{u_*} = \frac{1}{\kappa}\ln \overline{y} + B_o + \frac{\overline{a}}{\kappa \overline{y}} \tag{7.3}$$

Equations 7.2 and 7.3 are useful for three reasons: First, they are an excellent approximation to the overlap solutions for values of $y^+ > 2|a^+|$ (or $\overline{y} > 2|\overline{a}|$). Second, they are easier to incorporate into a composite solution which includes the viscous sublayer than is the overlap solution itself since they do not have the singularity at $y^+ = -a^+$ (cf. George and Castillo 1997). Third, the inner variable version can be shown to offer a useful insight into the role of the parameter a^+ as accounting for the mesolayer identified in the previous section.

In the overlap region (as noted earlier), the turbulence energy balance reduces to production equals dissipation; i.e., in inner variables, $P^+ \approx \epsilon^+$. This is exactly true in the limit of infinite Reynolds number, but is approximately true even at finite Reynolds numbers for $30 < y^+ < 0.1R^+$. The overlap solutions for the velocity, Reynolds stress and dissipation have already been obtained in the preceding sections. It follows immediately by substitution for P^+ and ϵ^+ that

$$P^+ = \frac{B_{i12}}{\kappa(y^+ + a^+)} = \epsilon^+ = \frac{E_i}{(y^+ + a^+)} \tag{7.4}$$

It is immediately obvious that the offset parameter a^+ must be the same for both velocity and dissipation, as *assumed* earlier. Hence $E_i = B_{i12}/\kappa \rightarrow 1/\kappa$, at least in the limit as $R^+ \rightarrow \infty$ since $B_{i12} \rightarrow 1$.

Therefore (as noted earlier), in this limit the dissipation and velocity derivative profiles are identical and equal to the derivative of equation 3.17 with respect to y^+; i.e.,

$$\epsilon^+ = \frac{1}{\kappa(y^+ + a^+)} = \epsilon_o^+ f_T(y^+) \tag{7.5}$$

where

$$\epsilon_o^+ \equiv \frac{1}{\kappa y^+} \tag{7.6}$$

and

$$f_T \equiv \left[1 + \frac{a^+}{y^+}\right]^{-1} \approx 1 - \frac{a^+}{y^+} \tag{7.7}$$

where the higher terms in the expansion in a^+ have been neglected. But this is identical to the form used by many turbulence modelers for wall-bounded flows (cf. Reynolds 1976, Hanjalic and Launder 1974) to account *empirically* for the change in the character of the dissipation near the wall since $R_t \approx 18y^+$ as noted earlier. Thus the interpretation of a^+ as a mesolayer parameter is obvious since it, in effect, modifies the dissipation (and hence the velocity profile) near the wall.

A similar form of f_T is obtained if the power law profile of George and Castillo (1997) for the boundary layer is expanded, even though the form of ϵ_o is different. However, interestingly, if the order of argument is reversed and any of the simple dissipation models (e.g., Reynolds 1976) are used to deduce the mesolayer contribution to the velocity profile for the boundary layer, they produce a $y^{+^{-1}}$ additive instead of the $y^{+^{\gamma-1}}$ required. Obviously these simple turbulence models, as currently posed, are consistent with the theory developed herein only for homogeneous flows, although the difference is slight.

Note that the common practice of choosing the model constants in equation 7.7 to produce a log profile at $y^+ \approx 30$ is clearly wrong if the theory proposed herein is correct, since this is approximately the location where the mesolayer only *begins*. As noted in Section 6, the mesolayer ends about $y^+ = 300$ and the inertial sublayer begins. It follows a^+ should be chosen to "turn-off" the low Reynolds number contribution about here (for increasing y^+) and "turn-on" the $\ln y$ solution.

8. The Superpipe Velocity Data

Now that the approximate region of validity of the overlap solution has been established as $30 < y^+ < 0.1R^+$ it is possible to test the theoretical profiles and the proposed model for the Reynolds number dependence. If they are correct, only an independent determination of either B_i or B_o is necessary to completely specify the profile, the rest of the parameters having been determined from the friction data. Since the very high Reynolds number superpipe experiments have a substantial range satisfying the conditions for the existence of the inertial sublayer ($300 < y^+ < 0.1R^+$), it should be possible to establish the value of B_i (or B_o) independent from the mesolayer. Also it should be possible to determine whether the parameter a^+ accounts for the mesolayer behavior, at least for those data sets where data are available below $y^+ = 300$. As shown below, both of these are indeed the case.

For all of the data sets it appears $B_i = 6.5$ is nearly optimal (at least for values of $R^+ > 850$, the lowest available from the superpipe experiment), so that for the remainder of this paper it will be assumed that $B_i = B_{i\infty}$. This value is very close to the value of 6.3 determined by Zagarola and Smits (1996a) by assuming κ fixed at 0.44. Since the difference, $B_{i\infty} - B_{o\infty} = 8.45$, was established from the friction data, it follows immediately that $B_{o\infty} = -1.95$. (Note, however, that the DNS channel data below suggest that $B_{o\infty} = -2.1$ and $B_{i\infty} = 6.35$ might be more appropriate, but the evidence is not conclusive yet.)

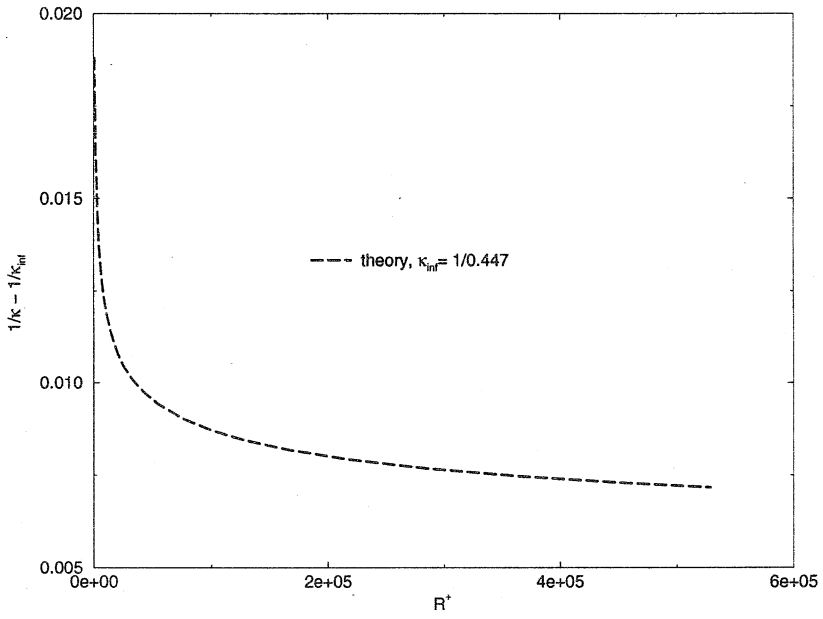

FIGURE 5. Variation of $1/\kappa - 1/\kappa_\infty$ with R^+, $\kappa_\infty = 0.447$

The constancy of B_i implies that it is B_o which shows all the Reynolds number dependence of the difference given by equation 4.8. Figures 5 and 6 show the theoretical variation of $1/\kappa$ and B_o with Reynolds number (equations 4.1 and 4.2). Clearly both converge very slowly to their asymptotic values. This slow approach has far more rel-

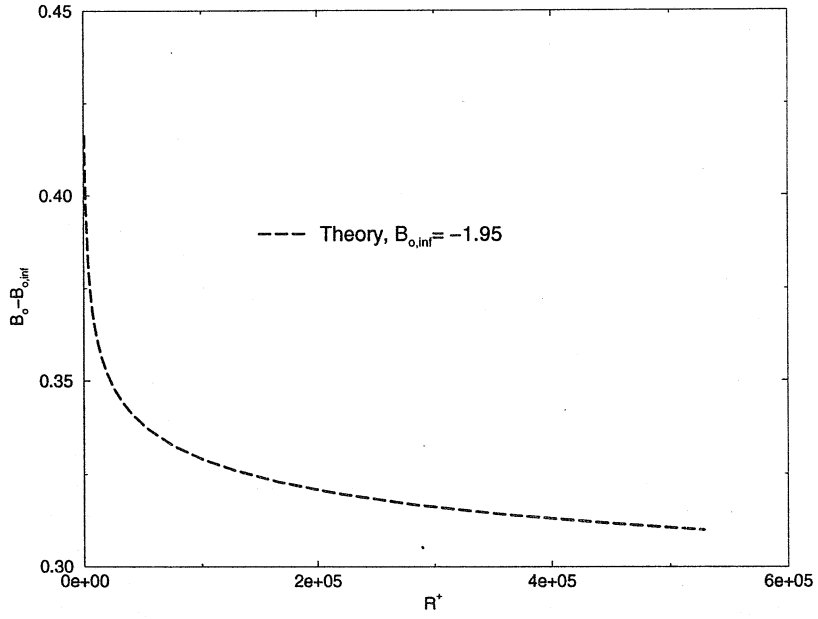

FIGURE 6. Variation of $B_o - B_{o\infty}$ with R^+, $B_{o\infty} = 8.50$

ative effect on B_o than it does on $1/\kappa$, however, since B_o has achieved only 85% of its asymptotic value at $R^+ = 10^5$. The observed variation of $1/\kappa$ and B_o and the constancy of B_i can be contrasted with the boundary layer results of George et al. 1996 and George and Castillo 1997 in which C_o, the outer coefficient was nearly constant while the power exponent γ and the inner coefficient C_i varied over the entire range of Reynolds numbers available.

The relative behavior of B_o and B_i means that the outer profile scaling shows more variation with Reynolds number in the overlap region than does the inner where only κ varies. This undoubtedly explains a great deal of the problems historically in establishing what $B_{o\infty}$ is and in determining whether the outer scaling is correct. And it might also explain the conclusion of Zagarola and Smits (1996) that a different scale for the outer flow is required, especially if attention is focussed on the overlap region instead of the core region of the flow.

Figures 7 and 8 show representative velocity profiles of the superpipe data at high and low Reynolds numbers respectively. The profiles scaled in inner variables are shown in the upper plots, and the same data scaled in outer variables is shown in the lower plots. Also shown for each profile are the overlap solutions of equations 3.16 and 3.17 together with equations 4.7 and 4.8. The vertical lines on each profile show the suggested bounds for the two sublayers of the overlap region; in particular, the mesolayer ($30 < y^+ < 300$ or $30/R^+ < \overline{y} < 300/R^+$) and the inertial sublayer ($300 < y^+ < 0.1R^+$ or $300/R^+ < \overline{y} < 0.1$). Note that because of the varying Reynolds number, the limits depending on R^+ are different for each profile. Note also that for the highest Reynolds number plots the data were not measured close enough to the wall to see any of the mesolayer; however they do show clearly the inertial sublayer. For the lowest Reynolds numbers, enough of the near wall region was resolved to see clearly the mesolayer, but the extent of the

inertial sublayer was limited or non-existent. The theoretical profiles were computed using the measured value of R^+ and assuming $a^+ = 0$, -8, and -16 (or $\overline{a} = 0$, $-8/R^+$, and $-16/R^+$). As noted above, the value of $B_{o\infty} = -1.95$ is determined since $B_{i\infty}$ has been chosen as 6.5 and $B_{i\infty} - B_{o\infty} = 8.45$ was established from the friction data earlier. Therefore there are *no* adjustable parameters in the outer scaled plot if a^+ is determined from the inner. Thus these outer profiles provide a completely independent test of the theory (and the data as well).

The value of $a^+ = 0$ corresponds to the inertial sublayer solution only, and as expected describes the data well only in the range of $300 < y^+ < 0.15R^+$. The boundary layer value of $a^+ = -16$ (from the power law) is clearly too large, but then there is no reason to expect it to be the same since the homogeneous pipe and inhomogeneous boundary layer flows are fundamentally different, at least in the outer and overlap regions. The best fit to the DNS channel flow data (see below) above $y^+ \approx 30$ is also $a^+ = -8$. It is possible to fit the data to substantially lower values of y^+ by using different values of a^+, but there appears to be no theoretical justification for doing so. Note that the Pitot tube used to make the pipe velocity measurements could be as much as much as two percent too high at $y^+ = 30$ because of the local turbulence intensity there (since $U_{meas}/U \approx 1 + [< u^2 > + < v^2 > + < w^2 >]/2U^2$). Hence, more confidence can be placed in the DNS data than in the low Reynolds number pipe flow measurements near and inside $y^+ = 30$. In spite of this, the agreement between experiment and theory over the entire overlap range is particularly gratifying since the velocity data were only used to establish B_i and a^+, the remaining parameters having been entirely determined by the friction data.

It is easy to see how the deviations from the log law due to the mesolayer contribution of a^+ could be viewed as a separate and distinct region. For example, Zagarola and Smits (1996) argue that the region $50 < y^+ < 500$ is described by a 1/7 power law with a coefficient of 8.7, and not their logarithmic profile (with constant coefficients) which fits the inner solution between $500 < y^+ < 0.1R^+$. If a power law is fitted to data generated by the overlap profile proposed herein using the constants determined above, it produces almost exactly the same 1/7-power and 8.7 coefficient over the same range. Thus it is clear that the same phenomenon is being described.

9. Channel versus Pipe Flow

Although both fully-developed channel and pipe flows are homogeneous in the streamwise direction and both scale with u_*, there is no reason, in principle, to expect the outer flow or overlap profiles of channel flow to be the same as for pipe flow. The former is planar and homogeneous in planes parallel to the surface, while the latter is axially symmetric. However, in spite of the fact that the geometries are different, the averaged equations for each flow are nearly the same, differing only in the turbulence and viscous transport terms.

The inner regions of both flows have long been known to be quite close (v. Monin and Yaglom 1971). In fact, they must be exactly the same in the limit as the ratio of the extent of the viscous sublayer to the pipe radius (or channel half-width) diminishes to zero, and this always happens in the limit of infinite Reynolds number. Therefore it is reasonable *to hypothesize* that the inner regions of both flows be the same. Then the only differences between channel and pipe flows must appear in the outer flow. If this is true, then all of the parameters governing the *inner* region (including the overlap region in inner variables) must be the same for both pipe and channel flows. In particular, the parameters κ and B_i must be the same, *as well as their dependence on Reynolds number.*

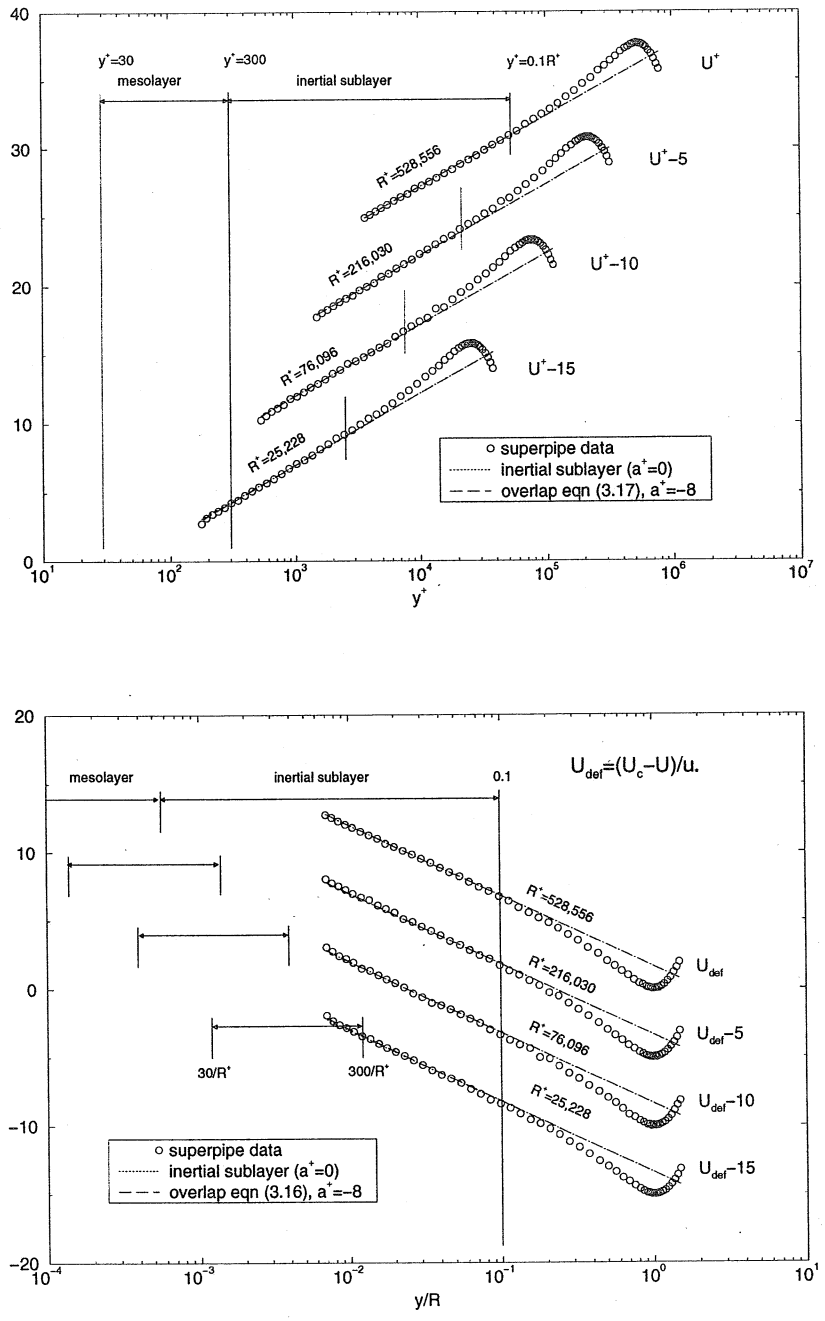

FIGURE 7. Inner and outer profiles at relatively high Reynolds number

Hence even the empirical constants A and α must be identical. Only the parameter B_o and the scale constant D_s can be different. Moreover, since equation 3.20 must be satisfied, *the channel flow value of B_o can at most differ by an additive constant from the pipe flow value*, since any other difference would affect the Reynolds number-dependent relation between κ and $B_i - B_o$.

Figure 9 shows the mean velocity profile data from the channel flow simulations of Kim et al. (1987) and Kim (1989) at values of $R^+ = 180$ and 395, where R in this case is taken to mean the channel half-width. Also shown is the as yet unpublished profile of Kim (1997) at $R^+ = 595$.† As before the profiles scaled in inner variables are presented in the upper figure, and the same data in outer variables in the lower. By the criteria established earlier, there should be no region which is described by a simple logarithmic profile alone without the mesolayer contribution, even at the highest Reynolds number. In fact, as is clear from the vertical lines on the plots, there should not even be a mesolayer region in the lowest Reynolds number profile (since $0.1R^+ < 30$).

Nonetheless, the theoretical overlap solution, equation 3.17, *with exactly the parameter values used above for the superpipe data* fits all three sets of data in inner variables nicely over the very limited range $30 < y^+ < 0.1R^+$. (In fact, the theoretical curve appears to work well to values of y^+ substantially closer to the wall even though its use below $y^+ = 30$ can not be justified theoretically, at least by the arguments presented earlier.) It is not even necessary to adjust the scale factor D_s which was chosen as unity, just as for the pipe data. This agreement is all the more remarkable because all of the constants have been obtained from the superpipe experiment and at much higher Reynolds number.

The theoretical outer velocity profile uses the pipe values for all constants except for $B_{o\infty}$ as noted above. Since $B_{o\infty}$ is quite small for the channel flow, even small uncertainties about its value have a relatively large effect on the outer profile. Therefore the approach taken here has been to first determine $B_{i\infty} - B_{o\infty}$ from the channel friction data, then use the value of $B_{i\infty}$ from the superpipe (since they should be the same as noted above) to determine $B_{o\infty}$ for the channel. Thus the channel flow velocity data scaled in outer variables provide a completely independent test of the theory. Unlike the superpipe data, however, there is much less DNS data available so a sophisticated optimization is not possible. However, there is only a single parameter which needs to be determined. Note that the experimental channel flow data has been avoided entirely because of uncertainties about the shear stress (v. Kim et al. 1987).

The best overall fit to the friction data, U_c/u_*, is achieved by choosing $B_{i\infty} - B_{o\infty} = 7.0$ with the relative errors being 0.18%, 0.57%, and 1.2% for the Reynolds numbers of 595, 395, and 180 respectively. It follows that $B_{o\infty} = -0.5$.

As shown in the lower figure of Figure 9, equation 3.16 provides a reasonable fit to the higher Reynolds number profiles over same region as for the inner scaling. The fit is especially impressive since there has been no effort to optimize the fit to the velocity profile data. (Recall that all constants but one were determined by the superpipe and even the remaining one was chosen from the friction data!) A near perfect fit (not shown) to the two higher Reynolds number profiles can be achieved, however, by using $B_{o\infty} = -0.65$, but the friction estimates increase to 0.089%, 1.3%, and 2.0% respectively if B_i is maintained at 6.5. On the other hand, if the value of $B_{i\infty}$ is reduced to 6.35, then both the better friction prediction and the better outer profiles fits can be maintained simultaneously (since $B_{i\,\mathrm{inf}} - B_{o\infty} = 7.0$ is maintained), but with little relative change to the inner profile. Note that such a value for B_i would be very close to the value of 6.3 suggested by Zagarola and Smits (1996). The authors have resisted the urge to

† The authors are very grateful to Professor Kim for making this data available to us.

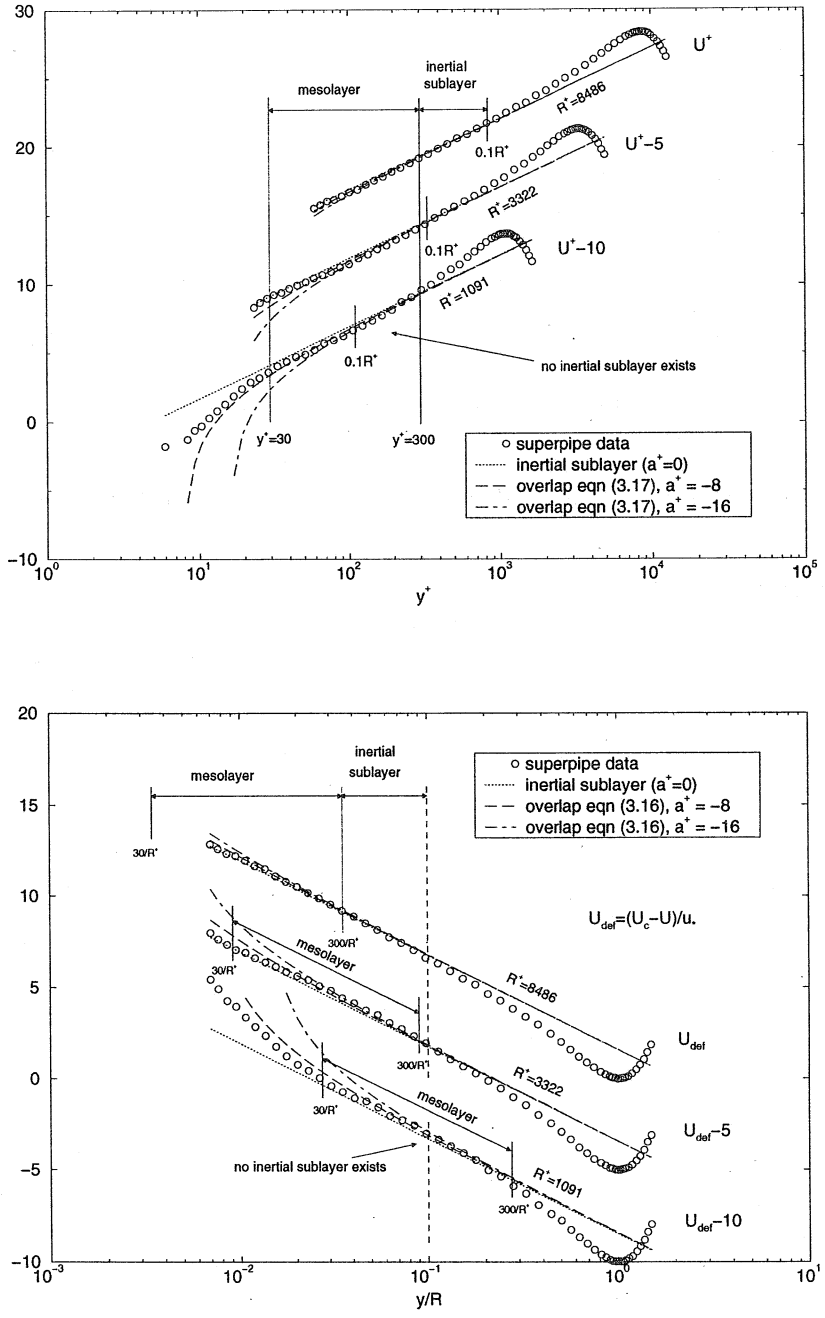

FIGURE 8. Inner and outer profiles at relatively low Reynolds number

re-analyze the pipe flow data until higher Reynolds number DNS data confirm the need to do so, but it is clear that the only other effect would be to change the pipe flow value of $B_{o\infty}$ from -1.95 to -2.1 which would scarcely be noticeable in the plots.

All of the errors between the calculated and DNS values of U_c/u_* are within the uncertainty of the DNS data itself which is estimated at one to two percent. The reason for the larger discrepancy between the lower Reynolds number profiles is probably that the theory is simply being stretched to Reynolds numbers below where it can reasonably be expected to apply. (As noted above, there is not even a region satisfying the conditions for an overlap in the $R^+ = 180$ profile since $0.1R^+ < 30$!) Regardless of the reason, it is clear that the value of $B_{o\infty}$ is substantially lower for the channel than for the pipe, but this was expected since, as noted above, the differences between the two flows should show up here. Moreover, also as expected, this appears to be the only place these differences show up.

The success of the theory developed herein in accounting for the channel flow data using the pipe flows constants should give considerable confidence in the entire theoretical approach. Moreover, it provides an independent confirmation of the values of the constants and the empirical function utilized for the Reynolds number dependence.

10. Summary and Conclusions

The Asymptotic Invariance Principle and the deductions from Near-Asymptotics, together with the recognition of the existence of a mesolayer, have provided an excellent description of the mean velocity and skin friction data from fully-developed channel and pipe flows over more than three and a half decades in Reynolds number. Specifically the theory describes the velocity profile in the region $30 < y^+ < 0.1R^+$ (or $30/R^+ < \overline{y} < 0.1$) for the superpipe experiment ($850 < R^+ < 530,000$) and the low Reynolds number DNS data as well ($R^+ = 180$, 395 and 595). Of the six parameters needed to describe the flow, four could be determined only from the friction data *only*. Three of these ($\kappa_\infty = 0.447$, $A = -0.67$ and $\alpha = 0.44$) were determined from the superpipe experiment alone, but probably apply to any *stream-wise homogeneous* wall-bounded flow. The difference parameter which appears in the friction law, $B_{i\infty} - B_{o\infty}$, is different for pipes and channels (even though $B_{i\infty}$ is the same). From the superpipe experiment, $B_{i\infty} - B_{o\infty} = 8.45$, while from the DNS channel data it was estimated to be 7.0. Both pipe and channel data sets were consistent with constant values of $B_i = B_{i\infty} = 6.5$ and $a^+ = -8$. It follows that the outer parameter $B_{o\infty} = -1.95$ for the pipe flow, and -0.5 for the channel flow. A case can also be made that the limiting values of $B_{o\infty}$ should be -2.1 and -0.65 corresponding to $B_\infty = 6.35$, but a final decision can probably not be made until higher Reynolds number DNS data becomes available.

Unlike the boundary layer where both Reynolds number effects and the mesolayer were of equal importance in understanding the data, for pipe and channel flows the Reynolds number dependence was found to be slight. In fact, only B_o shows significant variation over the range of the data, and then only about 5%. The von Karman parameter, κ, variation was only about 1%; and both B_i and a^+ were constant to within the accuracy of the data.

On the other hand, the mesolayer concept (and a^+ in particular) proved crucial in understanding where the theory applied and in understanding why previous attempts to verify the log law were less than totally satisfactory. In particular, the overlap mean velocity profile was found to not be a simple logarithm in y, but instead a logarithm in $y + a$. The most important consequence of this is that attempts to establish $\ln y$ behavior using velocity profile data inside $y^+ = 300$ are doomed to failure and the

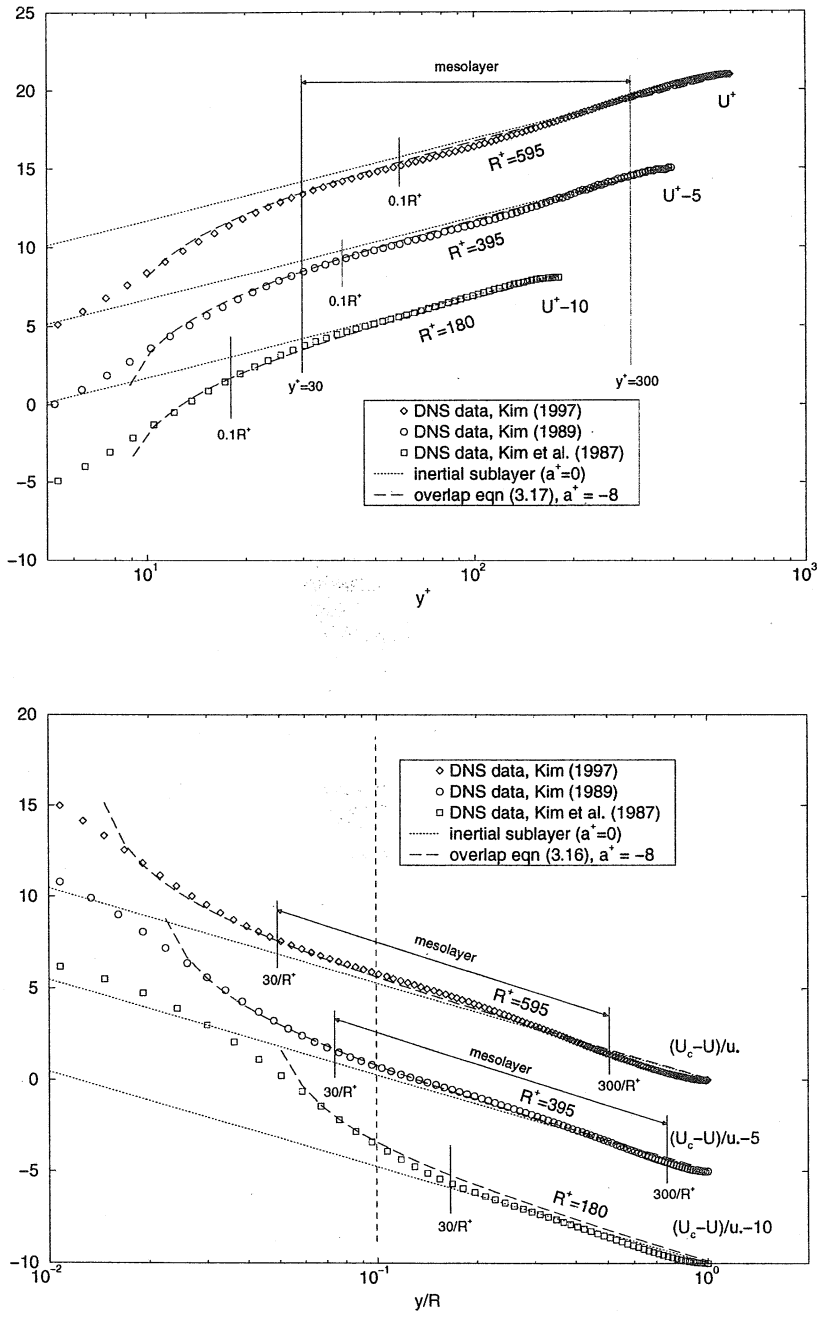

FIGURE 9. Channel flow DNS data of Kim et al. (1987), Kim (1989) and Kim (1997).

results misleading unless the mesolayer (and a in particular) are explicitly accounted for. This, of course, explains much of the confusion in the literature about precisely what the log parameters were and where the theory applied — not only was the wrong profile being used, but it was being applied to the wrong region.

It should be noted that for their boundary layer data analysis, George et al. 1996 and George and Castillo 1997 used a procedure which was the reverse of that used here. There a series of careful attempts was first made to obtain directly the variation of the parameters from the velocity profiles, then the friction law was inferred and shown to be in agreement with direct measurements. The fact that the procedure followed here has been equally successful lends credibility to both analyses, especially in view of the importance of the subtle difference between the friction law proposed here and a simple log law with constant coefficients.

There are a number of interesting questions which remain. One of these is whether the mesolayer parameter a^+ is indeed constant as it appears that it might be. This will require accurate measurements of the velocity profile near $y^+ = 30$ at considerably higher Reynolds numbers than has been possible to-date. Note that the problem is not with the overall flow Reynolds number (which in the superpipe was certainly adequate), but with the inability to resolve the flow near the wall at the higher Reynolds numbers due to probe size limitations. An obvious solution is a bigger pipe so less absolute resolution is required at a given Reynolds number — a Mega-Pipe perhaps (or maybe a Mighty Duct!).

Another question arises from the Reynolds number dependence itself which is nearly negligible for the channel and pipe flows, but crucial for the boundary layer flows. Is this a subtle consequence of the homogeneity of the former and inhomogeneity of the latter, or is it simply a reflection of the differing inner and outer velocity scales for the boundary layer with the consequent Reynolds number dependence? Or are these the same thing?

Then there is the fact that the parameter, α, which accounts for the Reynolds number dependence is nearly the same as for the boundary layer, and tantalizingly close to κ_∞ and the boundary layer value of $1/(\gamma_\infty C_{o\infty})$. The possible universality of these is particularly interesting, especially given the agreement between theory and experiment for both the homogeneous and inhomogeneous flows. A consequence of this is that the dissipation profiles for the pipe and the *infinite* Reynolds number boundary layer are nearly identical throughout the overlap region, even though they differ substantially for the finite Reynolds numbers of experiments. And, of course, this raises the whole question of the functions H (for the pipe and channel) and h (for the boundary layer) which contain the essential Reynolds number dependence of the flow: Can they (or alternatives) be derived directly from the underlying physics of the flow, perhaps through symmetry considerations of the turbulence dissipative scales or from the multi-point equations?

In conclusion, unlike the classical boundary layer theory which was shown by George and Castillo (1997) to be fundamentally flawed, the same approach has been able to show that the classical theory for pipe and channel flows is really pretty good. The present analysis has, from purely deductive reasoning using the Reynolds-averaged Navier-Stokes equations, been able to identify why the classical results were not totally successful, and also to account for both the recent DNS and superpipe observations. Thus it would seem that the Navier-Stokes equations indeed apply to turbulence, hardly a novel idea to most, but reassuring nonetheless.

11. Acknowledgments

The authors are particularly grateful to J. Kim, L. Smits, and M. Zagarola for making their work available to us, and also to M. Oberlack for helping us understand the need for the origin shift in the overlap analysis. The invitation to participate in the *Disquisitiones Mechanicae 1996* at the University of Illinois, Department of Theoretical and Applied Mechanics did much to focus our thinking and move this work forward. The efforts of Professors R. Adrian, S. Balachandar, R. Moser and especially H. Aref to organize and host it are greatly appreciated.

REFERENCES

Barenblatt, G.J. (1978) *Similarity, Self-similarity, and Intermediate Asymptotics*, Plenum, NY.

Barenblatt, G.J. (1993) Scaling laws for fully developed shear flow. Part 1, Basic hypotheses and analysis. *J. Fluid Mech.*, vol. 248, 513 –520.

Barenblatt, G.J. and Prostokishnin, V.M. (1993) Scaling laws for fully developed shear flow. Part 2, Processing of Experimental Data. *J. Fluid Mech.*, vol. 248, 513 –520.

Cole, J.D. and Kevorkian, J. (1981) *Perturbation Methods in Applied Mathematics*, Springer, NY.

Gad-el-Hak, M. and Bandyopadhyay, P.R. (1994) Reynolds Number Effects in Wall-Bounded Flows, *Applied Mech. Rev., 47*, 307 –3365.

George, W.K. (1990) ASCE Mtg, San Diego.

George, W.K. (1989) Self-Preservation of Turbulent Flows and Its Relation to Initial Conditions and Coherent Structures, in *Advances in Turbulence* (George and Arndt, eds.), 39 – 73, Hemisphere, NY.

George, W.K. (1995) Some New Ideas for Similarity of Turbulent Shear Flows, *Proc. of Lisbon Conf. on Turbulence and Turbulent Heat Transfer*, Hanjalic and Pereira, eds., Elsevier, Amsterdam.

George, W.K. and Bower,D (1988) APS/DFD Meeting, Buffalo, NY.

George, W.K., Castillo, L. and Knecht, P. (1992) The Zero-Pressure Gradient Boundary Layer Revisited, *13th Symposium on on Turbulence* (Reed, X.B., ed.), Rolla, Mo.

George, W.K., Castillo, L. and Knecht, P. (1996) The Zero-Pressure Gradient Boundary Layer, Turbulence Research Lab. Rept. 153, SUNY/Buffalo, Buffalo, NY. (available from http://www.eng.buffalo.edu/Research/trl/papers)

Frisch, U. (1995) *Turbulence: The Legacy of A.N. Kolmogorov*, C.U.P. Cambridge, UK.

George, W.K. and Castillo, L. (1993) Boundary Layers with Pressure Gradient: Another Look at the Equilibrium Boundary Layer, *Near Wall Turbulent Flows*, (So, R.M.C. et al. editors), 901 – 910, Elsevier, NY.

George, W.K. and Castillo, L. (1997) The Zero-Pressure-Gradient Turbulent Boundary Layer, *Appl. Mech. Reviews, 50*, 12, Pt.1, 689 –729 .

Gibson, M.M. private communication to WKG.

Hanjalic, K. and B.E. Launder (1974) Contribution towards a Reynolds stress closure for low-Reynolds number turbulence, Imp.Coll. Rept. HTS/74/24.

Kim, J., Moin, P. and Moser, R.T. (1987) Turbulence statistics in fully developed channel flow at low Reynolds number, *J. Fluid Mech., 177*, 133 – 166.

Kim, J. (1989) On the structure of pressure fluctuations in simulated turbulent channel flow, *J. Fluid Mech., 205*, 421 – 451.

Kim, J. (1997) private communication.

Long, R.R. (1976) presentation at Naval Hydrodynamics Mtg., Wash., DC., June.

Long, R.R. and Chen, T.-C. (1981) Experimental Evidence for the Existence of the 'Mesolayer' in Turbulent Systems, *J. Fluid Mech.*, 105, 19 – 59.

Monin, A.S. and Yaglom, A.M. (1971) *Statistical Fluid Mechanics*, MIT Press, Cambridge, MA.

Millikan, C.M. (1938) A critical discussion of turbulent flows in channels and circular tubes, *Proc. 5th Int. Congr. Appl. Mech.*, 386 – 392, Wiley, NY.

Oberlack, M. (1996) Lie Group Analysis of Turbulent Shear Flow, submitted for publication.

Panton, R.(1990) Scaling Turbulent Wall Layers *J. Fluids Engr., 112*, 425 – 432.

Perry, A.E. and Abell, C.J. (1975) J. Fluid Mech.,67, 257.

Prandtl, L. (1932) Zur Turbulenten Strömung in Rohren und längs Platten, *Ergeb. Aerod. Versuch Göttingen*, IV Lieferung, 18.

Reynolds, W.C. (1976) Computation of Turbulent Flows, Ann. Rev. of Fluid Mech., 8, 183 –208.

Stanton, T.E. and Pannell, J.R.(1914) Similarity of motion in relation to the surface friction of fluids, *Phil. Trans. Roy. Soc. A*, 214, p 199.

Tennekes, H. and Lumley, J.L. (1972) *A First Course in Turbulence*, MIT, Cambridge.

Tennekes, H. (1968) Outline of a Second-Order Theory of Turbulent Pipe Flow,*AIAA Jour.*, 6, 1735 – 1740.

Zagorola, M.V. (1996) Ph.D Dissertation, Princeton U.

Zagorola, M.V. and Smits, A.J. (1996) Scaling of the mean velocity profile for turbulent pipe flow. draft document.

List of Recent TAM Reports

No.	Authors	Title	Date
784	Sayre, T. L., and D. N. Riahi	Effect of rotation on flow instabilities during solidification of a binary alloy—*International Journal of Engineering Science* **34**, 1631–1645 (1996)	Feb. 1995
785	Xin, Y.-B., and K. J. Hsia	A technique to generate straight surface cracks for studying the dislocation nucleation condition in brittle materials—*Acta Metallurgica et Materialia* **44**, 845–853 (1996)	Mar. 1995
786	Riahi, D. N.	Finite bandwidth, long wavelength convection with boundary imperfections: Near-resonant wavelength excitation—*International Journal of Mathematics and Mathematical Sciences* **21**, 171–182 (1997)	Mar. 1995
787	Turner, J. A., and R. L. Weaver	Average response of an infinite plate on a random foundation—*Journal of the Acoustical Society of America* **99**, 2167–2175 (1996)	Mar. 1995
788	Weaver, R. L., and D. Sornette	The range of spectral correlations in pseudointegrable systems: GOE statistics in a rectangular membrane with a point scatterer—*Physical Review E* **52**, 341 (1995)	Apr. 1995
789	Students in TAM 293–294	Thirty-second student symposium on engineering mechanics, J. W. Phillips, coordinator: Selected senior projects by K. F. Anderson, M. B. Bishop, B. C. Case, S. R. McFarlin, J. M. Nowakowski, D. W. Peterson, C. V. Robertson, and C. E. Tsoukatos	Apr. 1995
790	Figa, J., and C. J. Lawrence	Linear stability analysis of a gravity-driven Newtonian coating flow on a planar incline	May 1995
791	Figa, J., and C. J. Lawrence	Linear stability analysis of a gravity-driven viscosity-stratified Newtonian coating flow on a planar incline	May 1995
792	Cherukuri, H. P., and T. G. Shawki	On shear band nucleation and the finite propagation speed of thermal disturbances—*International Journal of Solids and Structures*, in press (1996)	May 1995
793	Harris, J. G.	Modeling scanned acoustic imaging of defects at solid interfaces—Chapter in *IMA Workshop on Inverse Problems in Wave Propagation*, eds. G. Chevant, G. Papanicolaou, P. Sacks and W. E. Symes, 237–258, Springer-Verlag, New York (1996)	May 1995
794	Sottos, N. R., J. M. Ockers, and M. J. Swindeman	Thermoelastic properties of plain weave composites for multilayer circuit board applications	May 1995
795	Aref, H., and M. A. Stremler	On the motion of three point vortices in a periodic strip—*Journal of Fluid Mechanics* **314**, 1–25 (1996)	June 1995
796	Barenblatt, G. I., and N. Goldenfeld	Does fully-developed turbulence exist? Reynolds number independence versus asymptotic covariance—*Physics of Fluids* **7**, 3078–3082 (1995)	June 1995
797	Aslam, T. D., J. B. Bdzil, and D. S. Stewart	Level set methods applied to modeling detonation shock dynamics—*Journal of Computational Physics*, **126**, 390–409 (1996)	June 1995
798	Nimmagadda, P. B. R., and P. Sofronis	The effect of interface slip and diffusion on the creep strength of fiber and particulate composite materials—Proceedings of the ASME Applied Mechanics Division **213**, 125–143 (1995)	July 1995
799	Hsia, K. J., T.-L. Zhang, and D. F. Socie	Effect of crack surface morphology on the fracture behavior under mixed mode loading—*ASTM Special Technical Publication* 1296, in press (1996)	July 1995
800	Adrian, R. J.	Stochastic estimation of the structure of turbulent fields—*Eddy Structure Identification*, ed. J. P. Bonnet, Springer: Berlin 145–196 (1996)	Aug. 1995
801	Riahi, D. N.	Perturbation analysis and modeling for stratified turbulence	Aug. 1995
802	Thoroddsen, S. T.	Conditional sampling of dissipation in high Reynolds number turbulence—*Physics of Fluids* **8**, 1333–1335	Aug. 1995
803	Riahi, D. N.	On the structure of an unsteady convecting mushy layer—*Acta Mechanica*, in press (1996)	Aug. 1995

List of Recent TAM Reports (cont'd)

No.	*Authors*	*Title*	*Date*
804	Meleshko, V. V.	Equilibrium of an elastic rectangle: The Mathieu–Inglis–Pickett solution revisited—*Journal of Elasticity* **40**, 207–238 (1995)	Aug. 1995
805	Jonnalagadda, K., G. E. Kline, and N. R. Sottos	Local displacements and load transfer in shape memory alloy composites	Aug. 1995
806	Nimmagadda, P. B. R., and P. Sofronis	On the calculation of the matrix–reinforcement interface diffusion coefficient in composite materials at high temperatures—*Acta Metallurgica et Materialia*, **44**, 2711–2716 (1996)	Aug. 1995
807	Carlson, D. E., and D. A. Tortorelli	On hyperelasticity with internal constraints—*Journal of Elasticity* **42**, 91–98 (1966)	Aug. 1995
808	Sayre, T. L., and D. N. Riahi	Oscillatory instabilities of the liquid and mushy layers during solidification of alloys under rotational constraint—*Acta Mechanica* **121** , 143–152 (1997)	Sept. 1995
809	Xin, Y.-B., and K. J. Hsia	Simulation of the brittle–ductile transition in silicon single crystals using dislocation mechanics	Oct. 1995
810	Ulysse, P., and R. E. Johnson	A plane-strain upper-bound analysis of unsymmetrical single-hole and multi-hole extrusion processes	Oct. 1995
811	Fried, E.	Continua described by a microstructural field—*Zeitschrift für angewandte Mathematik und Physik*, **47**, 168–175 (1996)	Nov. 1995
812	Mittal, R., and S. Balachandar	Autogeneration of three-dimensional vortical structures in the near wake of a circular cylinder	Nov. 1995
813	Segev, R., E. Fried, and G. de Botton	Force theory for multiphase bodies—*Journal of Geometry and Physics*, in press (1996)	Dec. 1995
814	Weaver, R. L.	The effect of an undamped finite-degree-of-freedom "fuzzy" substructure: Numerical solutions and theoretical discussion—*Journal of the Acoustical Society of America* **100**, 3159–3164 (1996)	Jan. 1996
815	Haber, R. B., C. S. Jog, and M. P. Bendsøe	A new approach to variable-topology shape design using a constraint on perimeter—*Structural Optimization* **11**, 1–12 (1996)	Feb. 1996
816	Xu, Z.-Q., and K. J. Hsia	A numerical solution of a surface crack under cyclic hydraulic pressure loading	Mar. 1996
817	Adrian, R. J.	Bibliography of particle velocimetry using imaging methods: 1917–1995—*Produced and distributed in cooperation with TSI, Inc., St. Paul, Minn.*	Mar. 1996
818	Fried, E., and G. Grach	An order-parameter based theory as a regularization of a sharp-interface theory for solid–solid phase transitions—*Archive for Rational Mechanics and Analysis*, in press (1996)	Mar. 1996
819	Vonderwell, M. P., and D. N. Riahi	Resonant instability mode triads in the compressible boundary-layer flow over a swept wing—*International Journal of Engineering Science*, in press (1997)	Mar. 1996
820	Short, M., and D. S. Stewart	Low-frequency two-dimensional linear instability of plane detonation—*Journal of Fluid Mechanics*, in press (1997)	Mar. 1996
821	Casagranda, A., and P. Sofronis	On the scaling laws for the consolidation of nanocrystalline powder compacts—Proceedings of the IUTAM Symposium on the Mechanics of Granular and Porous Materials (1996)	Apr. 1996
822	Xu, S., and D. S. Stewart	Deflagration-to-detonation transition in porous energetic materials: A comparative model study—*Journal of Fluid Mechanics*, in press (1997)	Apr. 1996
823	Weaver, R. L.	Mean and mean-square responses of a prototypical master/fuzzy structure—*Journal of the Acoustical Society of America*, in press (1996)	Apr. 1996
824	Fried, E.	Correspondence between a phase-field theory and a sharp-interface theory for crystal growth—*Continuum Mechanics and Thermodynamics*, in press (1997)	Apr. 1996
825	Students in TAM 293–294	Thirty-third student symposium on engineering mechanics, J. W. Phillips, coordinator: Selected senior projects by W. J. Fortino II, A. A. Mordock, and M. R. Sawicki	May 1995

List of Recent TAM Reports (cont'd)

No.	Authors	Title	Date
826	Riahi, D. N.	Effects of roughness on nonlinear stationary vortices in rotating disk flows—*Mathematical and Computer Modeling*, in press (1996)	June 1996
827	Riahi, D. N.	Nonlinear instabilities of shear flows over rough walls	June 1996
828	Weaver, R. L.	Multiple scattering theory for a plate with sprung masses: Mean and mean-square responses	July 1996
829	Moser, R. D., M. M. Rogers, and D. W. Ewing	Self-similarity of time-evolving plane wakes	July 1996
830	Lufrano, J. M., and P. Sofronis	Enhanced hydrogen concentrations ahead of rounded notches and cracks—Competition between plastic strain and hydrostatic constraint	July 1996
831	Riahi, D. N.	Effects of surface corrugation on primary instability modes in wall-bounded shear flows	Aug. 1996
832	Bechel, V. T., and N. R. Sottos	Measuring debond length in the fiber pushout test—Proceedings of the ASME Mechanics and Materials Conference (1996)	Aug. 1996
833	Riahi, D. N.	Effect of centrifugal and Coriolis forces on chimney convection during alloy solidification—*Journal of Crystal Growth* **179** , 287–296 (1997)	Sept. 1996
834	Cermelli, P., and E. Fried	The influence of inertia on configurational forces in a deformable solid—*Proceedings of the Royal Society of London A*, in press (1996)	Oct. 1996
835	Riahi, D. N.	On the stability of shear flows with combined temporal and spatial imperfections	Oct. 1996
836	Carranza, F. L., B. Fang, and R. B. Haber	An adaptive space–time finite element model for oxidation-driven fracture	Nov. 1996
837	Carranza, F. L., B. Fang, and R. B. Haber	A moving cohesive interface model for fracture in creeping materials	Nov. 1996
838	Balachandar, S., R. Mittal, and F. M. Najjar	Properties of the mean wake recirculation region in two-dimensional bluff body wakes—*Journal of Fluid Mechanics*, in press (1997)	Dec. 1996
839	Ti, B. W., W. D. O'Brien, Jr., and J. G. Harris	Measurements of coupled Rayleigh wave propagation in an elastic plate	Dec. 1996
840	Phillips, W. R. C.	On finite-amplitude rotational waves in viscous shear flows	Jan. 1997
841	Riahi, D. N.	Direct resonance analysis and modeling for a turbulent boundary layer over a corrugated surface—*Acta Mechanica*, in press (1998)	Jan. 1997
842	Liu, Z.-C., R. J. Adrian, C. D. Meinhart, and W. Lai	Structure of a turbulent boundary layer using a stereoscopic, large format video-PIV	Jan. 1997
843	Fang, B., F. L. Carranza, and R. B. Haber	An adaptive discontinuous Galerkin methods for viscoplastic analysis	Jan. 1997
844	Xu, S., T. D. Aslam, and D. S. Stewart	High-resolution numerical simulation of ideal and non-ideal compressible reacting flows with embedded internal boundaries	Jan. 1997
845	Zhou, J., C. D. Meinhart, S. Balachandar, and R. J. Adrian	Formation of coherent hairpin packets in wall turbulence	Feb. 1997
846	Lufrano, J. M., P. Sofronis, and H. K. Birnbaum	Elastoplastically accommodated hydride formation and embrittlement	Feb. 1997
847	Keane, R. D., N. Fujisawa, and R. J. Adrian	Unsteady non-penetrative thermal convection from non-uniform surfaces	Feb. 1997

List of Recent TAM Reports (cont'd)

No.	*Authors*	*Title*	*Date*
848	Aref, H., and M. Brøns	On stagnation points and streamline topology in vortex flows	Mar. 1997
849	Asghar, S., T. Hayat, and J. G. Harris	Diffraction by a slit in an infinite porous barrier	Mar. 1997
850	Shawki, T. G., H. Aref, and J. W. Phillips	Mechanics on the Web—Proceedings of the International Conference on Engineering Education (Aug. 1997, Chicago)	Apr. 1997
851	Stewart, D. S., and J. Yao	The normal detonation shock velocity–curvature relationship for materials with non-ideal equation of state and multiple turning points	Apr. 1997
852	Fried, E., A. Q. Shen, and S. T. Thoroddsen	Traveling waves, standing waves, and cellular patterns in a steadily forced granular medium	Apr. 1997
853	Boyland, P. L., H. Aref, and M. A. Stremler	Topological fluid mechanics of stirring	Apr. 1997
854	Parker, S. J., and S. Balachandar	Viscous and inviscid instabilities of flow along a streamwise corner	May 1997
855	Soloff, S. M., R. J. Adrian, and Z.-C. Liu	Distortion compensation for generalized stereoscopic particle image velocimetry—*Measurement Science and Technology* **8**, 1–14 (1997)	May 1997
856	Zhou, Z., R. J. Adrian, S. Balachandar, and T. M. Kendall	Mechanisms for generating coherent packets of hairpin vortices in near-wall turbulence	June 1997
857	Neishtadt, A. I., D. L. Vainshtein, and A. A. Vasiliev	Chaotic advection in a cubic Stokes flow	June 1997
858	Weaver, R. L.	Ultrasonics in an aluminum foam	July 1997
859	Riahi, D. N.	High gravity convection in a mushy layer during alloy solidification	July 1997
860	Najjar, F. M., and S. Balachandar	Low-frequency unsteadiness in the wake of a normal flat plate	Aug. 1997
861	Short, M.	A parabolic linear evolution equation for cellular detonation instability	Aug. 1997
862	Short, M., and D. S. Stewart	Cellular detonation stability—I: A normal-mode linear analysis	Sept. 1997
863	Carranza, F. L., and R. B. Haber	A numerical study of intergranular fracture and oxygen embrittlement in an elastic–viscoplastic solid	Oct. 1997
864	Sakakibara, J., and R. J. Adrian	Whole-field measurement of temperature in water using two-color laser-induced fluorescence	Oct. 1997
865	Riahi, D. N.	Effect of surface corrugation on convection in a three-dimensional finite box of fluid-saturated porous material	Oct. 1997
866	Baker, C. F., and D. N. Riahi	Three-dimensional flow instabilities during alloy solidification	Oct. 1997
867	Fried, E.	Introduction (only) to *The Physical and Mathematical Foundations of the Continuum Theory of Evolving Phase Interfaces* (book containing 14 seminal papers dedicated to Morton E. Gurtin)	Oct. 1997
868	Folguera, A., and J. G. Harris	Coupled Rayleigh surface waves in a slowly varying elastic waveguide	Oct. 1997
869	Stewart, D. S.	Detonation shock dynamics: Application for precision cutting of metal with detonation waves	Oct. 1997
870	Shrotriya, P., and N. R. Sottos	Creep and relaxation behavior of woven glass/epoxy substrates for multilayer circuit board applications	Nov. 1997
871	Riahi, D. N.	Boundary wave–vortex interaction in channel flow at high Reynolds numbers	Nov. 1997
872	George, W. K., L. Castillo, and M. Wosnik	A theory for turbulent pipe and channel flows	Nov. 1997